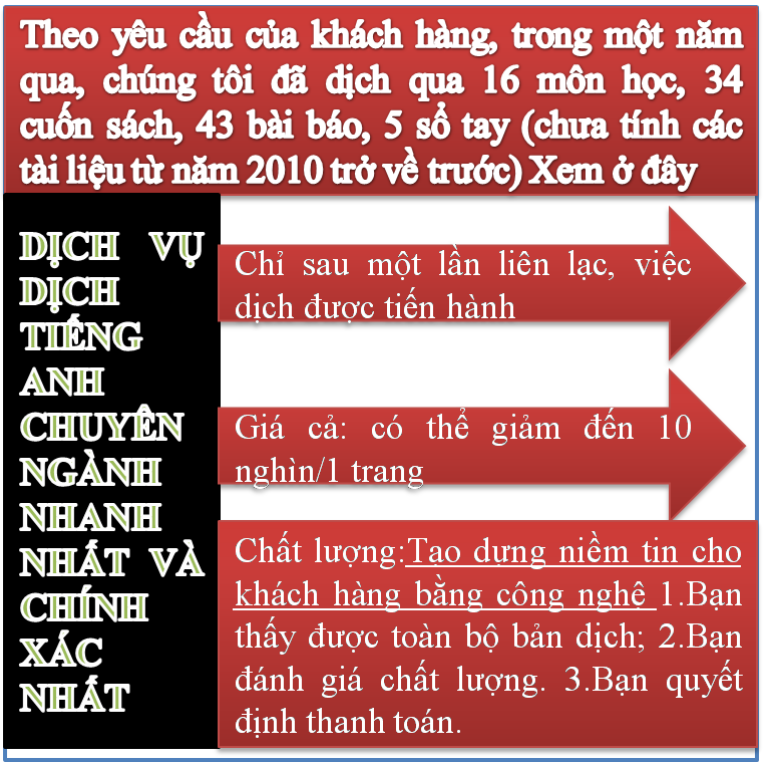

Tài liệu này được dịch sang tiếng việt bởi:

www.mientayvn.com

Tìm bản gốc tại thư mục này (copy link và dán hoặc nhấn Ctrl+Click):

https://drive.google.com/folderview?id=0B4rAPqlxIMRDSFE2RXQ2N3FtdDA&usp=sharing

Liên hệ để mua:

thanhlam1910_2006@yahoo.com hoặc frbwrthes@gmail.com hoặc số 0168 8557 403 (gặp Lâm)

Giá tiền: 1 nghìn /trang đơn (trang không chia cột); 500 VND/trang song ngữ

Dịch tài liệu của bạn: http://www.mientayvn.com/dich_tieng_anh_chuyen_nghanh.html

Friction stir welding and processing R.S. Mishraa'*, Z.Y. Mab

Abstract

Friction stir welding (FSW) is a relatively new solid-state joining process. This joining technique is energy efficient, environment friendly, and versatile. In particular, it can be used to join high-strength aerospace aluminum alloys and other metallic alloys that are hard to weld by conventional fusion welding. FSW is considered to be the most significant development in metal joining in a decade. Recently, friction stir processing (FSP) was developed for microstructural modification of metallic materials. In this review article, the current state of understanding and development of the FSW and FSP are addressed. Particular emphasis has been given to: (a) mechanisms responsible for the formation of welds and microstructural refinement, and (b) effects of FSW/FSP parameters on resultant microstructure and final mechanical properties. While the bulk of the information is related to aluminum alloys, important results are now available for other metals and alloys. At this stage, the technology diffusion has significantly outpaced the fundamental understanding of microstructural evolution and microstructure-property relationships.

1. Introduction

The difficulty of making high-strength, fatigue and fracture resistant welds in aerospace aluminum alloys, such as highly alloyed 2XXX and 7XXX series, has long inhibited the wide use of welding for joining aerospace structures. These aluminum alloys are generally classified as non-weldable because of the poor solidification microstructure and porosity in the fusion zone. Also, the loss in mechanical properties as compared to the base material is very significant. These factors make the joining of these alloys by conventional welding processes unattractive. Some aluminum alloys can be resistance welded, but the surface preparation is expensive,

Công nghệ gia công và hàn ma sát xoay R.S.Mishraa*, Z.Y .Mab

Tóm tắt

Hàn ma sát xoay (FSW) là một quá trình hàn nối trạng thái rắn tương đối mới. Kỹ thuật hàn nối này hiệu quả về mặt năng lượng(tiết kiệm năng lượng), thân thiện với môi trường, và linh hoạt. Đặc biệt, nó có thể được sử dụng để hàn các hợp kim nhôm có độ bền cao dùng trong hàng không vũ trụ và các hợp kim kim loại khác rất khó để hàn bằng kỹ thuật hàn nóng chảy thông thường. FSW được xem là bước phát triển quan trọng nhất trong kỹ thuật hàn kim loại trong một thập kỷ. Gần đây, gia công ma sát xoay (FSP) đã được phát triển để điều chỉnh vi cấu trúc của các vật liệu kim loại. Trong bài báo tổng quan này, chúng tôi phân tích (làm rõ) tiến trình nghiên cứu và phát triển FSW và FSP trong hiện tại. Đặc biệt chú trọng vào các vấn đề sau: (a) cơ chế đóng vai trò hình thành các mối hàn và sự tái kết tinh vi cấu trúc (kết tinh lại), và (b) ảnh hưởng của các tham số FSW / FSP đến các tính chất vi cấu trúc và tính chất cơ học cuối cùng. Trong khi phần lớn các thông tin có liên quan đến hợp kim nhôm, hiện tại các kết quả quan trọng về các kim loại và hợp kim khác đã có sẵn. Ở giai đoạn này, sự phổ biến công nghệ làm cho khả năng hiểu biết của chúng ta về mối quan hệ giữa sự tiến triển vi cấu trúc và các tính chất vi cấu trúc tăng nhanh đáng kể.

1. GIỚI THIỆU CHUNG:

Đã từ lâu, những khó khăn trong việc tạo ra các mối hàn có khả năng chống gãy, mỏi và có độ bên cao trong các hợp kim nhôm sử dụng trong hàng không vũ trụ, chẳng hạn như seri 2xxx và 7xxx hợp kim cao, làm cho chúng ta không thể sử dụng kỹ thuật hàn để hàn nối các cấu trúc hàng không vũ trụ. Nói chung, những hợp kim nhôm này thường được xếp vào loại không thể hàn vì vi cấu trúc ở trạng thái đông đặc nghèo và xốp trong vùng nóng chảy. Ngoài ra, sự mất mát các tính chất cơ học so với vật

with surface oxide being a major problem.	liệu nền rất đáng kể. Những yếu tố này làm cho việc hàn nối các hợp kim này bằng quá trình hàn thông thường không hấp dẫn (không được quan tâm nghiên cứu). Một số hợp kim nhôm có thể được hàn điện trở, nhưng việc chuẩn bị bề mặt đắt tiền, trong đó hiện tượng oxi hóa bề mặt là một khó khăn lớn.
Friction stir welding (FSW) was invented at The Welding Institute (TWI) of UK in 1991 as a solid state joining technique, and it was initially applied to aluminum alloys [1,2]. The basic concept of FSW is remarkably simple. A non-consumable rotating tool with a specially designed pin and shoulder is inserted into the abutting edges of sheets or plates to be joined and traversed along the line of joint (Fig. 1). The tool serves two primary functions: (a) heating of workpiece, and (b) movement of material to produce the joint. The heating is accomplished by friction between the tool and the workpiece and plastic deformation of workpiece. The localized heating softens the material around the pin and combination of tool rotation and translation leads to movement of material from the front of ……	Hàn ma sát xoay (FSW) được phát minh tại Viện hàn (TWI) của Vương quốc Anh vào năm 1991 như một kỹ thuật hàn nối trạng thái rắn, và ban đầu được áp dụng cho các hợp kim nhôm [1,2]. Ý tưởng của FSW cực kỳ đơn giản. Một công cụ quay với tốc độ không đổi có một chốt được thiết kế đặc biệt và trụ vai được chèn vào các cạnh tiếp giáp của các bảng hoặc tấm cần hàn và di chuyển dọc theo đường hàn (Hình 1).Công cụ này có hai chức năng chính: (a) làm nóng vật liệu hàn, và (b) di chuyển vật liệu để tạo ra mối hàn. Quá trình truyền nhiệt được thực hiện bởi ma sát giữa các công cụ và phôi (vật liệu cần hàn, vật liệu cần gia công) và sự biến dạng dẻo của vật liệu. Quá trình làm nóng cục bộ làm mềm các vật liệu xung quanh chốt và sự kết hợp giữa chuyển động quay và tịnh tiến của công cụ dẫn đến chuyển động của vật liệu từ phía trước .....
Fig. 1. Schematic drawing of friction stir welding.	Hình 1 Sơ đồ minh họa (sơ đồ kết cấu) hàn ma sát xoay.
the pin to the back of the pin. As a result of this process a joint is produced in ‘solid state’. Because of various geometrical features of the tool, the material movement around the pin can be quite complex [3]. During FSW process, the material undergoes intense plastic deformation at elevated temperature, resulting in generation of fine and equiaxed recrystallized grains [4-7]. The fine micmstn.icri.ne in friction stir welds produces good mechanical properties.	chốt đến phía sau chốt. Kết quả của quá trình này là một mối hàn được tạo ra ở "trạng thái rắn". Do tính chất đa dạng về hình dạng công cụ, sự di chuyển vật liệu quanh chốt khá phức tạp [3]. Trong quá trình FSW, vật liệu trải qua quá trình biến dạng dẻo mãnh liệt ở nhiệt độ cao, dẫn đến sự tạo các hạt mịn và tái kết tinh đẳng trục [4-7]. Tính chất vi cấu trúc tốt của các mối hàn ma sát xoay tạo ra các tính chất cơ học tốt.
FSW is considered to be the most significant development in metal joining in a decade and is a ‘‘green’’ technology due to its energy efficiency, environment friendliness, and versatility. As compared to the conventional welding methods, FSW	FSW được xem là sự phát triển quan trọng nhất trong công nghệ hàn kim loại trong một thập kỷ và là một công nghệ "xanh" do tính hiệu quả về mặt năng lượng, thân thiện với môi trường, và

consumes considerably less energy. No cover gas or flux is used, thereby making the process environmentally friendly. The joining does not involve any use of filler metal and therefore any aluminum alloy can be joined without concern for the compatibility of composition, which is an issue in fusion welding. When desirable, dissimilar aluminum alloys and composites can be joined with equal ease [8-10]. In contrast to the traditional friction welding, which is usually performed on small axisymmetric parts that can be rotated and pushed against each other to form a joint [11], friction stir welding can be applied to various types of joints like butt joints, lap joints, T butt joints, and fillet joints [12]. The key benefits of FSW are summarized in Table 1.

Recently friction stir processing (FSP) was developed by Mishra et al. [13,14] as a generic tool for microstructural modification based on the basic principles of FSW. In this case, a rotating tool is inserted in a monolithic workpiece for localized microstructural modification for specific property enhancement. For example, high-strain rate superplasticity was obtained in commercial 7075Al alloy

……
……..

Table 1
Key benefits of friction stir welding
Metallurgical benefits Environmental benefits Energy benefits

Solid phase process Low distortion of workpiece Good dimensional stability and repeatability

No loss of alloying elements

Excellent metallurgical properties in the joint area

tính linh hoạt. So với các phương pháp hàn thông thường, FSW tiêu thụ năng lượng ít hơn đáng kể. Không cần khí phủ hoặc dòng khí, do đó làm cho quá trình thân thiện với môi trường. Quá trình hàn nối không cần kim loại phụ gia và do đó bất kỳ hợp kim nhôm nào cũng có thể được hàn mà không cần quan tâm đến khả năng tương thích của các thành phần, nhưng điều này lại quan trọng trong hàn nóng chảy. Nếu muốn, các hợp kim nhôm không giống nhau và composite có thể được hàn với mức độ dễ như nhau [8-10]. Trái ngược với hàn ma sát truyền thống, là một quá trình thường được thực hiện trên các bộ phận đối xứng trục nhỏ có thể được quay và được đẩy vào nhau để tạo thành một mối hàn [11], hàn ma sát xoay có thể được áp dụng cho nhiều loại mối hàn khác nhau như các mối hàn đầu tiếp đầu, mối hàn nối ghép chồng, mối hàn ghép chữ T, và mối hàn góc [12]. Các lợi ích chính của FSW được tóm tắt trong Bảng 1.

Gần đây, gia công ma sát xoay (FSP) được phát triển bởi Mishra và các cộng sự. [13,14] như một công cụ tổng quát hóa để điều chỉnh vi cấu trúc dựa trên các nguyên tắc cơ bản của FSW. Trong trường hợp này, một công cụ quay được lắp vào một phôi đơn khối để điều chỉnh vi cấu trúc cục bộ để tăng cường một tính chất cụ thể nào đó. Ví dụ, vật liệu siêu dẻo tốc độ biến dạng cao đã thu được dưới dạng hợp kim 7075Al thương mại

.....

[redacted]

Fine microstructure
Absence of cracking

Replace multiple parts joined by fasteners

No shielding gas required
No surface cleaning required
Eliminate grinding wastes
Eliminate solvents required for degreasing

Consumable materials saving, such as rugs, wire or any other gases
Improved materials use (e.g., joining different thickness) allows reduction in weight
Only 2.5% of the energy needed for a laser weld

Decreased fuel consumption in light weight aircraft, automotive and ship applications

……
……..

by FSP [13-15]. Furthermore, FSP technique has been used to produce surface composite on aluminum substrate [16], homogenization of powder metallurgy aluminum alloy [17], microstructural modification of metal matrix composites [18] and property enhancement in cast aluminum alloys [19].

FSW/FSP is emerging as a very effective solid-state joining/processing technique. In a relatively short duration after invention, quite a few successful applications of FSW have been demonstrated [20-23]. In this paper, the current state of understanding and development of the FSW and FSP are reviewed.

2. Process parameters

FSW/FSP involves complex material movement and plastic deformation. Welding parameters, tool geometry, and joint design exert significant effect on the material flow pattern and temperature distribution, thereby influencing the microstructural

evolution of material. In this section, a few major factors affecting FSW/FSP process, such as tool geometry, welding parameters, joint design are addressed.

2.1. Tool geometry

Tool geometry is the most influential aspect of process development. The tool geometry plays a critical role in material flow and in turn governs the traverse rate at which FSW can be conducted. An FSW tool consists of a shoulder and a pin as shown schematically in Fig. 2. As mentioned earlier, the tool has two primary functions: (a) localized heating, and (b) material flow. In the initial stage of tool plunge, the heating results primarily from the friction between pin and workpiece. Some additional heating results from deformation of material.

The tool is plunged till the shoulder touches the workpiece. The friction between the shoulder and workpiece results in the biggest component of heating. From the heating aspect, the relative size of pin and shoulder is important, and the other design features are not critical. The shoulder also provides confinement for the heated volume of material. The second function of the tool is to ‘stir’ and ‘move’ the material. The uniformity of microstructure and properties as well as process loads are governed by the tool design. Generally a concave shoulder and threaded cylindrical pins are used.

With increasing experience and some improvement in understanding of material flow, the tool geometry has evolved significantly. Complex features have been added to alter material flow, mixing and reduce process loads. For example, WhorlTM and MX Triflute™ tools developed by TWI are

…….

Featureless Shoulder Scrolled Shoulder (viewed from

underneath)
Fig. 2. Schematic drawing of the FSW tool.
……
…….

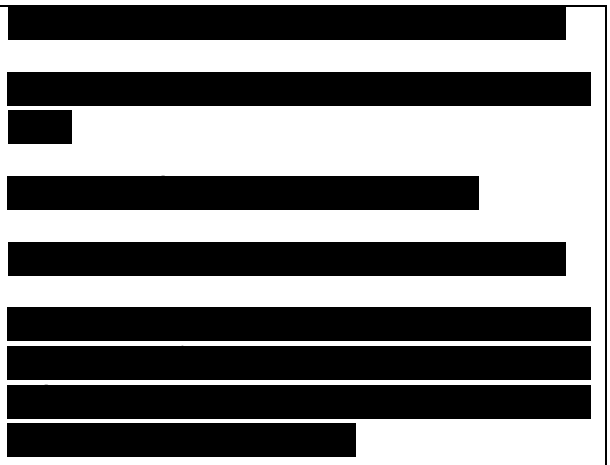

Fig. 3. WorlTM and MX TrifluteTM tools developed by The Welding Institute (TWI), UK (Copyright© 2001, TWI Ltd) (after Thomas et al. [24]).

shown in Fig. 3. Thomas et al. [24] pointed out that pins for both tools are shaped as a frustum that displaces less material than a cylindrical tool of the same root diameter. Typically, the WhorlTM reduces the displaced volume by about 60%, while the MX Triflute™ reduces the displaced volume by about 70%. The design features of the Whorl™ and the MX Triflute™ are believed to (a) reduce welding force, (b) enable easier flow of plasticized material, (c) facilitate the downward augering effect, and (d) increase the interface between the pin and the plasticized material, thereby increasing heat generation.

It has been demonstrated that aluminum plates with a thickness of up to 50 mm can be successfully friction stir welded in one pass using these two tools. A 75 mm thick 6082Al-T6 FSW weld was made using Whorl™ tool in two passes, each giving about 38 mm penetration. Thomas et al. [24] suggested that the major factor determining the superiority of the whorl pins over the conventional cylindrical pins is the ratio of the swept volume during rotation to the volume of the pin itself, i.e., a ratio of the ‘‘dynamic volume to the static volume’’ that is important in providing an adequate flow path. Typically, this ratio for pins with similar root diameters and pin length is 1.1:1 for conventional cylindrical pin, 1.8:1 for the Whorl™ and 2.6:1 for the MX Triflute™ pin (when welding 25 mm thick plate).

For lap welding, conventional cylindrical threaded pin resulted in excessive thinning of the top sheet, leading to significantly reduced bend properties [25]. Furthermore, for lap welds, the width of the weld interface and the angle at which the notch meets the edge of the weld is also important for applications where fatigue is of main concern. Recently, two new pin geometries—Flared-Trifute™ with the flute lands being flared out (Fig. 4) and A-skew™ with the pin axis being slightly inclined to the axis of machine spindle (Fig. 5) were developed for improved quality of lap welding [25-27]. The design features of the Flared-TrifuteTM and the A-skewTM are believed to: (a) increase the ratio between of the swept volume and static volume of the pin, thereby improving the flow path around and underneath the pin, (b) widen the welding region due to flared-out flute lands in the Flared-TrifuteTM pin and the skew action in the A-skewTM pin, (c) provide an improved mixing action for oxide fragmentation and dispersal at the weld interface, and (d) provide an orbital forging action at the root of the weld due to the skew action, improving weld quality in this region. Compared to the

……
……

Fig. 4. Flared-Triflute™ tools developed by The Welding Institute (TWI), UK: (a) neutral flutes, (b) left flutes, and (c) right hand flutes (after Thomas et al. [25]).

conventional threaded pin, Flared-Trifute™ and A-skewTM pins resulted in: (a) over 100% improve¬ment in welding speed, (b) about 20% reduction in axial force, (c) significantly widened welding region (190-195% of the plate thickness for Flared-Trifute™ and A-skewTM pins, 110% for conventional threaded pin), and (d) a reduction in upper plate thinning by a factor of >4 [27]. Further, Flared-Trifute™ pin reduced significantly the angle of the notch upturn at the overlapping plate/weld interface, whereas A-skewTM pin produced a slight downturn at the outer regions of the overlapping plate/weld interface, which are beneficial to

improving the properties of the FSW joints [25,27]. Thomas and Dolby [27] suggested that both Flared-Trifute™ and A-skewTM pins are suitable for lap, T, and similar welds where joining interface is vertical to the machine axis.

Further, various shoulder profiles were designed in TWI to suit different materials and conditions (Fig. 6). These shoulder profiles improve the coupling between the tool shoulder and the workpieces by entrapping plasticized material within special re-entrant features.

Considering the significant effect of tool geometry on the metal flow, fundamental correlation between material flow and resultant microstructure of welds varies with each tool. A critical need is to develop systematic framework for tool design. Computational tools, including finite element analysis

Fig. 5. A-SkewTM tool developed by The Welding Institute (TWI), UK: (a) side view, (b) front view, and (c) swept region encompassed by skew action (after Thomas et al. [25]).

Fig. 6. Tool shoulder geometries, viewed from underneath the shoulder (Copyright© 2001, TWI Ltd) (after Thomas et al. [24]).

(FEA), can be used to visualize the material flow and calculate axial forces. Several companies have indicated internal R&D efforts in friction stir welding conferences, but no open literature is available on such efforts and outcome. It is important to realize

that generalization of microstructural development and influence of processing parameters is difficult in absence of the tool information.

2.2. Welding parameters

For FSW, two parameters are very important: tool rotation rate (v, rpm) in clockwise or counterclockwise direction and tool traverse speed (n, mm/min) along the line of joint. The rotation of tool results in stirring and mixing of material around the rotating pin and the translation of tool moves the stirred material from the front to the back of the pin and finishes welding process. Higher tool rotation rates generate higher temperature because of higher friction heating and result in more intense stirring and mixing of material as will be discussed later. However, it should be noted that frictional coupling of tool surface with workpiece is going to govern the heating. So, a monotonic increase in heating with increasing tool rotation rate is not expected as the coefficient of friction at interface will change with increasing tool rotation rate.

In addition to the tool rotation rate and traverse speed, another important process parameter is the angle of spindle or tool tilt with respect to the workpiece surface. A suitable tilt of the spindle towards trailing direction ensures that the shoulder of the tool holds the stirred material by threaded pin and move material efficiently from the front to the back of the pin. Further, the insertion depth of pin into the workpieces (also called target depth) is important for producing sound welds with smooth tool shoulders. The insertion depth of pin is associated with the pin height. When the insertion depth is too shallow, the shoulder of tool does not contact the original workpiece surface. Thus, rotating shoulder cannot move the stirred material efficiently from the front to the back of the pin, resulting in generation of welds with inner channel or surface groove. When the insertion depth is too deep, the shoulder of tool plunges into the workpiece creating excessive flash. In this case, a significantly concave weld is produced, leading to local thinning of the welded plates. It

should be noted that the recent development of 'scrolled' tool shoulder allows FSW with 0° tool tilt. Such tools are particularly preferred for curved joints.

Preheating or cooling can also be important for some specific FSW processes. For materials with high melting point such as steel and titanium or high conductivity such as copper, the heat produced by friction and stirring may be not sufficient to soften and plasticize the material around the rotating tool. Thus, it is difficult to produce continuous defect-free weld. In these cases, preheating or additional external heating source can help the material flow and increase the process window. On the other hand, materials with lower melting point such as aluminum and magnesium, cooling can be used to reduce

……
……..

Fig. 7. Joint con figurations for friction stir welding: (a) square butt, (b) edge butt, (c) T butt joint, (d) lap joint, (e) multiple lap joint, (f) T lap joint, and (g) fillet joint.

extensive growth of recrystallized grains and dissolution of strengthening precipitates in and around the stirred zone.

2.3. Joint design

The most convenient joint configurations for FSW are butt and lap joints. A simple square butt joint is shown in Fig. 7a. Two plates or sheets with same thickness are placed on a backing plate and clamped firmly to prevent the abutting joint faces from being forced apart. During the initial plunge of the tool, the forces are fairly large and extra care is required to ensure that plates in butt configuration do not separate. A rotating tool is plunged into the joint line and traversed along this line when the shoulder of the

tool is in intimate contact with the surface of the plates, producing a weld along abutting line. On the other hand, for a simple lap joint, two lapped plates or sheets are clamped on a backing plate.

A rotating tool is vertically plunged through the upper plate and into the lower plate and traversed along desired direction, joining the two plates (Fig. 7d). Many other configurations can be produced by combination of butt and lap joints. Apart from butt and lap joint configurations, other types of joint designs, such as fillet joints (Fig. 7g), are also possible as needed for some engineering applications.

It is important to note that no special preparation is needed for FSW of butt and lap joints. Two clean metal plates can be easily joined together in the form of butt or lap joints without any major concern about the surface conditions of the plates.

3. Process modeling

FSW/FSP results in intense plastic deformation and temperature increase within and around the stirred zone. This results in significant microstructural evolution, including grain size, grain boundary character, dissolution and coarsening of precipitates, breakup and redistribution of dispersoids, and texture. An understanding of mechanical and thermal processes during FSW/FSP is needed for optimizing process parameters and controlling microstructure and properties of welds. In this section, the present understanding of mechanical and thermal processes during FSW/FSP is reviewed.

3.1. Metal flow

The material flow during friction stir welding is quite complex depending on the tool geometry, process parameters, and material to be welded. It is of practical importance to understand the material flow characteristics for optimal tool design and obtain high structural efficiency welds. This has led to numerous investigations on material flow behavior during FSW. A number of approaches, such as tracer technique by marker, welding of dissimilar alloys/metals, have been used to visualize material flow pattern in FSW. In addition, some computational methods including FEA have been also used to model the material flow.

3.1.1. Experimental observations

The material flow is influenced very significantly by the tool design. Therefore, any general¬ization should be treated carefully. Also, most of the studies do not report tool design and all process conditions. Therefore, differences among various studies cannot be easily discerned. To develop an overall pattern, in this review a few studies are specifically summarized and then some general trends are presented.

3.1.1.1. Tracer technique by marker. One method of tracking the material flow in a friction stir weld is to use a marker material as a tracer that is different from the material being welded. In the past few years, different marker materials, such as aluminum alloy that etch differently from the base metal [28-30], copper foil [31], small steel shots [32,33], Al-SiCp and Al-W composites [3,34], and tungsten wire [35], have been used to track the material flow during FSW.

Reynolds and coworkers [28-30] investigated the material flow behavior in FSW 2195Al-T8 using a marker insert technique (MIT). In this technique, markers made of 5454Al-H32 were embedded in the path of the rotating tool as shown in Fig. 8 and their

final position after welding was revealed by milling off successive slices of 0.25 mm thick from the top surface of the weld, etching with Keller's reagent, and metallographic examination.

Further, a projection of the marker positions onto a vertical plane in the welding direction was constructed. These investigations revealed the following. First, all welds exhibited some common flow patterns. The flow was not symmetric about the weld centerline. Bulk of the marker material moved to a final position behind its original position and only a small amount of the material on the advancing side was moved to a final position in front of its original position. The backward movement of material was limited to one pin diameter behind its original position. Second, there is a well-defined interface between the advancing and retreating sides, and the material was not really stirred across the interface during the FSW process, at least not on a macroscopic level. Third, material was pushed downward on the advancing side and moved toward the top at the retreating side within the pin diameter. This indicates that the ''stirring'' of material occurred only at the top of the weld where the material transport was directly influenced by the rotating tool shoulder that moved material from the retreating side around the pin to the advancing

……

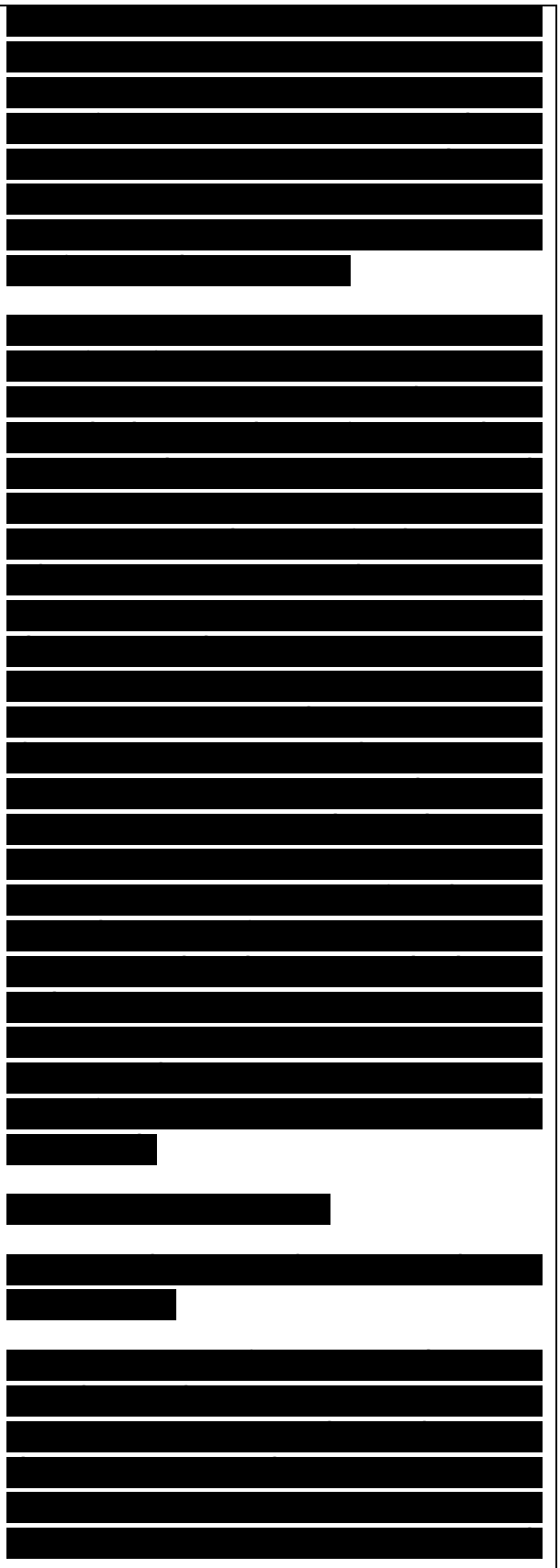

Fig. 8. Schematic drawing of the marker configuration (after Reynolds [29]).

side. Fourth, the amount of vertical displacement of the retreating side bottom marker was inversely proportional to the weld pitch (welding speed/rotation rate, i.e. the tool advance per rotation). Fifth, the material transport across the weld centerline increased with increasing the pin diameter at a constant tool rotation rate and traverse speed.

Based on these observations, Reynolds et al. [29,30] suggested that the friction stir welding process can be roughly described as an in situ extrusion process wherein the tool shoulder, the pin, the weld backing plate, and cold base metal outside the weld zone form an ‘‘extrusion chamber’’ which moves relative to the workpiece. They concluded that the extrusion around the pin combined with the stirring action at the top of the weld created within the pin diameter a secondary, vertical, circular motion around the longitudinal axis of the weld.

Guerra et al. [31] studied the material flow of FSW 6061Al by means of a faying surface tracer and a pin frozen in place at the end of welding. For this technique, weld was made with a thin 0.1 mm high-purity Cu foil along the faying surface of the weld. After a stable weld had been established, the pin rotation and specimen translation were manually stopped to produce a pin frozen into the workpiece. Plan view and transverse metallographic sections were examined after etching. Based on the microstructural examinations, Guerra et al. [31] concluded that the material was moved around the pin in FSW by two processes. First, material on the advancing side front of a weld entered into a zone that rotates and advances simultaneously with the pin. The material in this zone was very highly deformed and sloughed off behind the pin in arc shaped features. This zone exhibited high Vicker’s microhardness of 95.

Second, material on the retreating front side of the pin extruded between the rotational zone and the parent metal and in the wake of the weld fills in between material sloughed off from the rotational zone. This zone exhibited low Vicker’s microhardness of 35. Further, they pointed out that material near the top of the weld (approximately the upper one-third) moved under the influence of the shoulder rather than the threads on the pin.

Colligan [32,33] studied the material flow behavior during FSW of aluminum alloys by means of steel shot tracer technique and ‘‘stop action’’ technique. For the steel shot tracer technique, a line of small steel balls of 0.38 mm diameter were embedded along welding direction at different positions within butt joint welds of 6061Al-T6 and 7075Al-T6 plates. After stopping welding, each weld was subsequently radiographed to reveal the distribution of the tracer material around and behind the pin.

The ‘‘stop action’’ technique involved terminating friction stir welding by suddenly stopping the forward motion of the welding tool and simultaneously retracting the tool at a rate that caused the welding tool pin to unscrew itself from the weld, leaving the material within the threads of the pin intact and still attached to the keyhole. By sectioning the keyhole, the flow pattern of material in the region immediately within the threads of the welding tool was revealed. These investigations revealed the following important observations. First, the distribution of the tracer steel shots can be divided into two general categories: chaotical and continuous distribution. In the regions near top surface of the weld, individual tracer elements were scattered in an erratic way within a relatively broad zone behind the welding tool pin, i.e., chaotical distribution. The chaotically deposited tracer steel shots had moved to a greater depth from their original position. In other regions of the weld, the initial continuous line of steel shots was reorientated and deposited as a roughly continuous line of steel shot behind the pin, i.e., continuous distribution.

However, the tracer steel shots were found to be little closer to the upper surface of the weld. Second, in the leading side of the keyhole, the thread form gradually developed from curls of aluminum. The continuous downward motion of the thread relative to the forward advance of the pin caused the material captured inside the thread space to be deposited behind the pin. Based on these observations, Colligan [32,33] concluded that not all the material in the tool

path was actually stirred and rather a large amount of the material was simply extruded around the retreating side of the welding tool pin and deposited behind. However, it should be pointed out that if the marker material has different flow strength and density, it can create uncertainty about the accuracy of the conclusions.

London et al. [34] investigated material flow in FSW of 7050Al-T7451 monitored with 6061Al- 30vol.% SiCp and Al-20vol.% W composite markers. The markers with a cross-section of 0.79 mm x 0.51 mm were placed at the center on the midplane of the workpiece (MC) and at the advancing side on the midplane (MA). In each FSW experiment, the forward progress of the tool was stopped while in the process of spreading the marker. The distribution of marker material was examined by metallography and X-ray. Based on experimental observations, London et al. [34] suggested that the flow of the marker in the FSW zone goes through the following sequence of events.

First, material ahead of the pin is significantly uplifted because of the 3° tilt of the tool, which creates a ‘‘plowing action’’ of the metal ahead of the weld. Second, following this uplift, the marker is sheared around the periphery of the pin while at the same time it is being pushed downward in the plate because of the action of the threads. Third, marker material is dropped off behind the pin in ‘‘streaks’’ which correspond to the geometry of the threads and specific weld parameters used to create these welds. Furthermore, London et al. [34] showed that the amount of material deformation in the FSW weld depends on the locations relative to the pin. Markers on the advancing side of the weld are distributed over a much wider region in the wake of the weld than markers that begin at the weld centerline.

3.1.1.2. Flow visualization by FSW of dissimilar materials.

In addition to the tracer technique, several studies have used friction stir welding of dissimilar metals for visualizing the complex flow phenomenon. Midling [35] investigated the influence of the welding speed on the material flow in welds of dissimilar aluminum alloys. He was the first to report on interface shapes using images of the microstructure. However, information on flow visualization was limited to the interface between dissimilar alloys.

Ouyang and Kovacevic [36] examined the material flow behavior in friction stir butting welding of 2024Al to 6061Al plates of 12.7 mm thick. Three different regions were revealed in the welded zone. The first was the mechanically mixed region characterized by the relatively uniformly dispersed particles of different alloy constituents. The second was the stirring-induced plastic flow region consisting of alternative vortex-like lamellae of the two aluminum alloys. The third was the unmixed region consisting of fine equiaxed grains of the 6061Al alloy. They reported that in the welds the contact between different layers is intimate, but the mixing is far from complete. However, the bonding between the two aluminum alloys was complete. Further, they attributed the vortex-like structure and alternative lamellae to the stirring action of the threaded tool, in situ extrusion, and traverse motion along the welding direction.

Murr and co-workers [8,10,37,38] investigated the solid-state flow visualization in friction stir butt welding of 2024Al to 6061Al and copper to 6061Al. The material flow was described as a chaotic-dynamic intercalation microstructures consisting of vortex-like and swirl features. They further suggested that the complex mixing and intercalation of dissimilar metals in FSW is essentially the same as the microstructures characteristic of mechanically alloyed systems. On the other hand, a recent investigation on friction stir lap welding of 2195Al to 6061Al revealed that there is large vertical movement of material within the rotational zone caused by the wash and backwash of the threads [31]. Guerra et al. [31] have stated that material entering this zone followed an unwound helical trajectory formed by the

rotational motion, the vertical flow, and the translational motion of the pin.

3.1.1.3. Microstructural observations. The idea that the FSW is likened to an extrusion process is also supported by Krishnan [39]. Krishnan [39] investigated the formation of onion rings in friction stir welds of 6061Al and 7075Al alloys by using different FSW parameters. Onion rings found in the welded zone is a direct evidence of characteristic material transport phenomena occurring during FSW.

It was suggested that the friction stir welding process can be thought to be simply extruding one layer of semicylinder in one rotation of the tool and a cross-sectional slice through such a set of semicylinder results in the familiar onion ring structure. On the other hand, Biallas et al. [40] suggested that the formation of onion rings was attributed to the reflection of material flow approximately at the imaginary walls of the groove that would be formed in the case of regular milling of the metal.

The induced circular movement leads to circles that decrease in radii and form the tube system. In this case, it is believed that there should be thorough mixing of material in the nugget region. Although microstructural examinations revealed an abrupt variation in grain size and/or precipitate density at these rings [41,42], it is noted that the understanding of formation of onion rings is far from complete and an insight into the mechanism of onion ring formation would shed light on the overall material flow occurring during FSW.

Recently, Ma et al. [43] conducted a study on microstructural modification of cast A356 via friction stir processing. As-cast A356 plates were subjected

to friction stir processing by using different tool geometries and FSP parameters. Fig. 9 shows the optical micrographs of as-cast A356 and FSP sample prepared using a standard threaded pin and tool rotation rate of 900 rpm and traverse speed of 203 mm/min.

The as-cast A356 was characterized by coarse acicular Si particles with an aspect ratio of up to 25, coarse primary aluminum dendrites with an average size of ~100 mm, and porosity of ~50 mm diameter (Fig. 9a). The acicular Si particles were preferentially distributed along the boundaries of the primary aluminum dendrites, i.e., the distribution of Si particles in the as-cast A356 was not uniform. FSP resulted in a significant breakup of acicular Si particles and aluminum dendrites.

A uniform redistribution of the broken Si particles in the aluminum matrix was also produced. After FSP, the average aspect ratio of Si was reduced to ~2.0. Further, FSP also eliminated the porosity in the as-cast A356. Clearly, the material within the processed zone of the FSP A356 experienced intense stirring and mixing, thereby resulting in breakup of the coarse acicular Si particles and dendrite structure and homogeneous distribution of the Si particles throughout the aluminum matrix. Previous investigations have indicated that the extrusion at high temperature does not reduce the high-aspect-ratio reinforcements to nearly equiaxed particles [44,45]. Besides, as-extruded metal matrix composites are usually characterized by alternative particle-rich bands and particle-free bands [45,46]. Therefore, in the case of FSP A356 under the experimental conditions used, the material flow within the nugget zone cannot be considered as a simple extrusion process.

……
…….

Fig. 9. Optical micrographs showing the microstructure of as-cast and FSP A356 (standard

threaded pin, 900 rpm and 203 mm/min) [43].

3.1.2. Material flow modeling

Apart from experimental approaches, a number of studies have been carried out to model the materials flow during FSW using different computational codes [47-53], mathematical modeling tools [54,55], simple geometrical model [56], and metalworking model [57]. These attempts were aimed at understanding the basic physics of the material flow occurring during FSW.

Xu et al. [47] developed two finite element models, the slipping interface model and the frictional contact model, to simulate the FSW process. The simulation predictions of the material flow pattern based on these finite element models compare qualitatively well with an experimentally measured pattern by means of marker insert technique [29,30].

Colegrove and Shercliff [49] modeled the metal flow around profiled FSW tools using a two¬dimensional Computational Fluid Dynamics (CFD) code, Fluent. A 'slip' model was developed, where the interface conditions were governed by the local shear stresses. The two-dimensional modeling resulted in the following important findings.

First, flow behavior obtained by the slip model is significantly different from that obtained by the common assumption of material stick. The slip model revealed significant differences in flow with different tool shapes, which is not evident with the conventional stick model. Second, the deformation region for the slip model is much smaller on the advancing side than retreating side. Third, the material in the path of the pin is swept round the retreating side of the tool. This characteristic of the model is supported by flow visualization experiments by London et al. [3,34] and Guerra et al. [31]. Fourth, the streamlines show a bulge behind the tool, and the dragging of material behind the pin on the advancing

side. This correlated well with previous embedded marker experiments by Reynolds and co-workers [29,30]. Smith et al. [50] and Bendzsak and Smith [51] developed a thermo-mechanical flow model (STIR-3D). The principles of fluid mechanics were applied in this model. It assumes viscous heat dissipation as opposed to frictional heating. This model uses tool geometry, alloy type, tool rotation speed, tool position and travel speed as inputs and predicts the material flow profiles, process loads, and thermal profiles. It was indicated that three quite distinct flow regimes were formed below the tool shoulder, namely, (a) a region of rotation immediately below the shoulder where flow occurred in the direction of tool rotation, (b) a region where material is extruded past the rotating tool and this occurred towards the base of the pin, and (c) a region of transition in between regions (a) and (b) where the flow had chaotic behavior.	[redacted]

Askari et al. [52] adapted a CTH code [58] that is a three-dimensional code capable of solving time-dependent equations of continuum mechanics and thermodynamics. This model predicts important fields like strain, strain rate and temperature distribution. The validity of the model was verified by previous marker insert technique [3,34]. Goetz and Jata [53] used a two-dimensional FEM code, DEFORM [59], to simulate material flow in FSW of 1100Al and Ti-6Al-4V alloys. Non- isothermal simulation showed that highly localized metal flow is likely to occur during FSW. The movement of tracking points in these simulations shows metal flow around the tool from one side to the other, creating a weld. The simulations predict strain rates of 2-12 s_1 and strains of 2-5 in the zone of localized flow.	[redacted]
Stewart et al. [54] proposed two models for FSW process, mixed zone model and single slip surface model. Mixed zone model assumes that the metal in the plastic zone flows in a vortex system at an angular velocity of the tool at the tool-metal interface and the angular velocity drops to zero at the edge of the plastic zone. In the single slip surface model, the principal rotational slip takes place at a contracted slip surface outside the tool-workpiece interface. It was demonstrated that using a limited region of slip, predictions of the thermal field, the force and the weld region shape were in agreement with experimental measurement. Nunes [55] developed a detailed mathematical model of wiping flow transfer. This model is found to have the in-built capability to describe the tracer experiments.	[redacted]
Recently, Arbegast [57] suggested that the resultant microstructure and metal flow features of a friction stir weld closely resemble hot worked microstructure	[redacted]

of typical aluminum extrusion and forging. Therefore, the FSW process can be modeled as a metalworking process in terms of five conventional metal working zones: (a) preheat, (b) initial deformation, (c) extrusion, (d) forging, and (e) post heat/cool down (Fig. 10).	[redacted]
In the preheat zone ahead of the pin, temperature rises due to the frictional heating of the rotating tool and adiabatic heating because of the deformation of material. The thermal properties of material and the traverse speed of the tool govern the extent and heating rate of this zone. As the tool moves forward, an initial deformation zone forms when material is heated to above a critical temperature and the magnitude of stress exceeds the critical flow stress of the material, resulting in material flow.	[redacted]
The material in this zone is forced both upwards into the shoulder zone and downwards into the extrusion zone, as shown in Fig. 10. A small amount of material is captured in the swirl zone beneath the pin tip where a vortex flow pattern exists. In the extrusion zone with a finite width, material flows around the pin from the front to the rear. A critical isotherm on each side of the tool defines the width of the extrusion zone where the magnitudes of stress and temperature are insufficient to allow metal flow.	[redacted]
Following the extrusion zone is the forging zone where the material from the front of the tool is forced into the cavity left by the forward moving pin under hydrostatic pressure conditions. The shoulder of the tool helps to constrain material in this cavity and also applies a downward forging force.	[redacted]
Material from shoulder zone is dragged across the joint from the retreating side toward the advancing side. Behind the forging zone is the post heat/cool zone where the material cools under either passive or forced cooling conditions. Arbegast [57] developed a simple approach to metal flow modeling of the extrusion zone using mass balance considerations	[redacted]

that reveals a relationship between tool geometry, operating parameters, and flow stress of the materials being joined. It was indicated that the calculated temperature, width of the extrusion zone, strain rate, and extrusion pressure are consistent with experimental observations.

In summary, the material flow during FSW is complicated and the understanding of deformation process is limited. It is important to point out that there are many factors that can influence the material flow during FSW. These factors include tool geometry (pin and shoulder design, relative dimensions of pin and shoulder), welding parameters (tool rotation rate and direction, i.e., clockwise or counter¬clockwise, traverse speed, plunge depth, spindle angle), material types, workpiece temperature, etc. It is very likely that the material flow within the mắt điểm hàn during FSW consists of several independent deformation processes.

……
……

Fig. 10. (a) Metal flow patterns and (b) metallurgical processing zones developed during friction stir welding (after Arbegast [57]).

3.2. Temperature distribution

FSW results in intense plastic deformation around rotating tool and friction between tool and workpieces. Both these factors contribute to the temperature increase within and around the stirred zone. Since the temperature distribution within and around the stirred zone directly influences the microstructure of the welds, such as grain size, grain boundary character, sự tăng trưởng and dissolution of precipitates, and resultant mechanical properties of the welds, it is important to obtain information about temperature distribution during FSW. However, temperature measurements within the stirred zone are very difficult due to the intense plastic deformation produced by the rotation and translation of tool. Therefore, the maximum temperatures within the

stirred zone during FSW have been either estimated from the microstructure of the weld [4,5,60] or recorded by embedding thermocouple in the regions adjacent to the rotating pin [41,61-63].

An investigation of microstructural evolution in 7075Al-T651 during FSW by Rhodes et al. [4] showed dissolution of larger precipitates and reprecipitation in the đường trục hàn. Therefore, they concluded that maximum process temperatures are between about 400 and 480 °C in an FSW 7075Al-T651. On the hand, Murr and co-workers [5,60] indicated that some of the precipitates were not dissolved during welding and suggested that the temperature rises to roughly 400 °C in an FSW 6061Al. Recently, Sato et al. [61] studied the microstructural evolution of 6063Al during FSW using transmission electron microscopy (TEM) and compared it with that of simulated weld thermal cycles. They reported that the precipitates within the weld region (0-8.5 mm from đường trục hàn) were completely dissolved into aluminum matrix. By comparing with the microstructures of simulated weld thermal cycles at different peak temperatures, they concluded that the regions 0-8.5, 10, 12.5, and 15 mm away from the friction stir đường trục hàn were heated to temperatures higher than 402, 353, 302 °C and lower than 201 °C, respectively.

Recently, Mahoney et al. [41] conducted friction stir welding of 6.35 mm thick 7075Al-T651 plate and measured the temperature distribution around the stirred zone both as a function of distance from the stirred zone and through the thickness of the sheet. Fig. 11 shows the peak temperature distribution adjacent to the stirred zone. Fig. 11 reveals three important observations. First, maximum temperature was recorded at the locations close to the stirred zone, i.e., the edge of the stirred zone, and the temperature decreased with increasing distance from the stirred zone. Second, the temperature at

……

……

Fig. 11. Peak temperature distribution adjacent to a friction stir weld in 7075Al-T651. The line on the right side of figure shows the mắt điểm hàn boundary (after Mahoney et al. [41]).

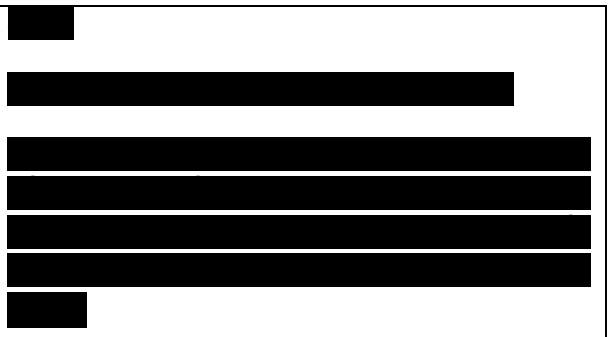

the edge of the stirred zone increased from the bottom surface of the plate to the top surface. Third, a maximum temperature of 475 °C was recorded near the corner between the edge of the stirred zone and the top surface. This temperature is believed to exceed the solution temperature for the hardening precipitates in 7075Al-T651 [64-66]. Based on these results the temperature within the stirred zone is likely to be above 475 °C. However, the maximum temperature within the stirred zone should be lower than the melting point of 7075Al because no evidence of material melting was observed in the weld [4,41].

More recently, an attempt was made by Tang et al. [62] to measure the heat input and temperature distribution within friction stir weld by embedding thermocouples in the region to be welded. 6061Al-T6 aluminum plates with a thickness of 6.4 mm were used. They embedded thermocouples in a series of small holes of 0.92 mm diameter at different distances from weld seam drilled into the back surface of the workpiece. Three depths of holes (1.59, 3.18, and 4.76 mm) were used to measure the temperature field at one quarter, one half, and three quarter of the plate thickness. They reported that the thermocouple at the đường trục hàn was not destroyed by the pin during welding but did change position slightly due to plastic flow of material ahead of the pin [62].

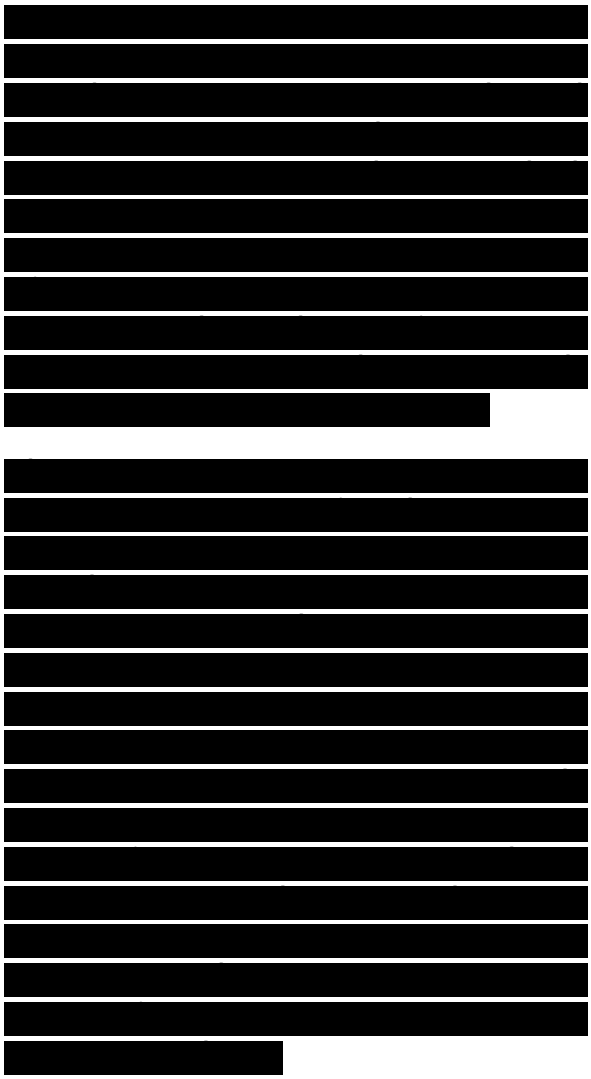

Fig. 12 shows the variation of the peak temperature with the distance from the đường trục hàn for various depths below the top surface. Three important observations can be made from this plot. First, maximum peak temperature was recorded at the đường trục hàn and with increasing distance from the đường trục hàn, the peak temperature decreased. At a tool rotation rate of 400 rpm and a traverse speed of 122 mm/min, a peak temperature of ~450 °C was

observed at the đường trục hàn one quarter from top surface. Second, there is a nearly isothermal region ~4 mm from the đường trục hàn. Third, the peak temperature gradient in the thickness direction of the welded joint is very small within the stirred zone and between 25 and 40 °C in the region away from the stirred zone. This indicates that the temperature distribution within the stirred zone is relatively uniform. Tang et al. [62] further investigated the effect of weld pressure and tool rotation rate on the temperature field of the weld zone. It was reported that increasing both tool rotation rate and weld pressure resulted in an increase in the weld temperature. Fig. 13 shows the effect of tool rotation rate on the peak temperature as a function of distance from the đường trục hàn. Clearly, within the weld zone the peak temperature increased by almost 40 °C with increasing tool rotation rate from 300 to 650 rpm, whereas it only increased by 20 °C when the tool rotation rate increased from 650 to 1000 rpm, i.e., the rate of temperature increase is lower at higher

……
……

Fig. 13. Effect of tool rotation rate on peak temperature as a function of distance from đường trục hàn for a 6061Al-T6 FSW weld made at 120 mm/min traverse speed (after Tang et al. [62]).

tool rotation rates. Furthermore, Tang et al. [62] studied the effect of shoulder on the temperature field by using two tools with and without pin. The shoulder dominated the heat generation during FSW (Fig. 14). This was attributed to the fact that the contact area and vertical pressure between the shoulder and workpiece is much larger than those between the pin and workpiece, and the shoulder has higher linear velocity than the pin with smaller radius [62]. Additionally, Tang et al. [62] showed that the thermocouples placed at equal distances from the weld seam but on opposite sides of the weld showed no significant differences in the temperature.

Similarly, Kwon et al. [63], Sato et al. [67], and Hashimoto et al. [68] also measured the temperature rise in the weld zone by embedding thermocouples in the regions adjacent to the rotating pin. Kwon et al. [63] reported that in FSW 1050Al, the peak temperature in the FSP zone increased linearly from 190 to 310 °C with increasing tool rotation rate from 560 to 1840 rpm at a constant tool traverse speed of 155 mm/min. An investigation by Sato et al. [67] indicated that in FSW 6063Al, the peak temperature of FSW thermal cycle increased sharply with increasing tool rotation rate from 800

……

Fig. 14. Variation of peak temperature with distance from đường trục hàn for a 6061Al-T6 FSW weld made with and without pin (400 rpm and 120 mm/min traverse speed) (after Tang et al. [62]).

to 2000 rpm at a constant tool traverse speed of 360 mm/min, and above 2000 rpm, however, it rose gradually with increasing rotation rate from 2000 to 3600 rpm. Peak temperature of >500 °C was recorded at a high tool rotation rate of 3600 rpm. Hashimoto et al. [68] reported that the peak temperature in the weld zone increases with increasing the ratio of tool rotation rate/traverse speed for FSW of 2024Al-T6, 5083Al-O and 7075Al-T6 (Fig. 15). A peak temperature >550 °C was observed in FSW 5083Al-O at a high ratio of tool rotation rate/traverse speed.

In a recent investigation, a numerical three-dimensional heat flow model for friction stir welding of age hardenable aluminum alloy has been developed by Frigaad et al. [69], based on the method

of finite differences. The average heat input per unit area and time according to their model is [69]:

…… (1)

where q0 is the net power (W), m the friction coefficient, P the pressure (Pa), v the tool rotational speed (rot/s) and R is the tool radius (m). Frigaad et al. [69] suggested that the tool rotation rate and shoulder radius are the main process variables in FSW, and the pressure P cannot exceed the actual flow stress of the material at the operating temperature if a sound weld without depressions is to be obtained. The process model was compared with in situ thermocouple measurements in and around the FSW zone. FSW of 6082Al-T6 and 7108Al-T79 was performed at constant tool rotation rate of 1500 rpm and a constant welding force of 7000 N, at three welding speeds of 300, 480, and 720 mm/min. They revealed three important observations. First, peak temperature of above ^500 °C was recorded in the FSW zone. Second, peak temperature decreased with increasing traverse speeds from 300 to 720 mm/ min. Third, the three-dimensional numerical heat flow model yields a temperature-time pattern that is consistent with that observed experimentally.

Similarly, three-dimensional thermal model based on finite element analysis developed by Chao and Qi [70] and Khandkar and Khan [71] also showed reasonably good match between the simulated temperature profiles and experimental data for both butt and overlap FSW processes.

The effect of FSW parameters on temperature was further examined by Arbegast and Hartley [72]. They reported that for a given tool geometry and depth of penetration, the maximum temperature was observed to be a strong function of the rotation rate (v, rpm) while the rate of heating was a strong function of the traverse speed (n, rpm). It was also noted that there was a slightly higher temperature on the advancing

side of the joint where the tangential velocity vector direction was same as the forward velocity vector. They measured the average maximum temperature on 6.35 mm aluminum plates as a function of the pseudo-‘‘heat index w (w = v2/v)”. It was demonstrated that for several aluminum alloys a general relationship between maximum welding temperature (T, °C) and FSW parameters (v, n) can be explained by

…… (2)

where the exponent a was reported to range from 0.04 to 0.06, the constant Kis between 0.65 and 0.75, and Tm (°C) is the melting point of the alloy. The maximum temperature observed during FSW of various aluminum alloys is found to be between 0.6Tm and 0.9Tm, which is within the hot working temperature range for those aluminum alloys. Furthermore, the temperature range is generally within the solution heat-treatment temperature range of precipitation-strengthened aluminum alloys.

Recently, Schmidt et al. [73] have developed an analytical model for the heat generation in FSW. The important difference between this model and the previous models is the choice of sticking and sliding contact conditions. The expressions for total heat generation for sticking, sliding, and partial sliding/sticking conditions, respectively, are

…….. (3a)

……(3b)

……. (3c)

where Q is the total heat generation (W), syield the yield strength (Pa), v the tool angular rotation rate (rad/s), Rshoulder the tool shoulder radius (m), Rprobe the tool probe radius (m), a the tool shoulder cone angle (°), Hprobe the tool probe height (m), p the contact pressure (Pa), and d is the contact state variable. Schmidt et al. [73] verified the model using 2024Al-T3 alloy. They noted that the analytical heat generation estimate correlates with the experimental heat generation. The experimental heat generation was not proportional to the experimental plunge

force. Based on this they suggested that sticking condition must be present at the tool/matrix interface. It should be noted, however, that the experiments were only performed at a rotational rate of 400 rpm and a welding speed of 120 mm/min.

In summary, many factors influence the thermal profiles during FSW. From numerous experi¬mental investigations and process modeling, we conclude the following. First, maximum temperature rise within the weld zone is below the melting point of aluminum. Second, tool shoulder dominates heat generation during FSW. Third, maximum temperature increases with increasing tool rotation rate at a constant tool traverse speed and decreases with increasing traverse speed at a constant tool rotation rate. Furthermore, maximum temperature during FSW increases with increasing the ratio of tool rotation rate/traverse speed. Fourth, maximum temperature rise occurs at the top surface of weld zone. Various theoretical or empirical models proposed so far present different pseudo-heat index. The experimental verification of these models is very limited and attempts to correlate various data sets

……..

Fig. 16. Variation of mắt điểm hàn cross-section area with pseudo-heat index [74].

with models for this review did not show any general trend. The overall picture includes frictional heating and adiabatic heating. The frictional heating depends on the surface velocity and frictional coupling (coefficient of friction). Therefore, the temperature generation should increase from center of the tool shoulder to the edge of the tool shoulder. The pin should also provide some frictional heating and this aspect has been captured in the model of Schmidt et al. [73]. In addition, the adiabatic heating is likely to be maximum at the pin and tool shoulder surface and decrease away from the interface. Currently, the

theoretical models do not integrate all these contributions. Recently, Sharma and Mishra [74] have observed that the mắt điểm hàn area changes with pseudo-heat index (Fig. 16). The results indicate that the frictional condition change from ‘stick’ at lower tool rotation rates to ‘stick/slip’ at higher tool rotation rates. The implications are very important and needs to be captured in theoretical and computational modeling of heat generation.

4. Microstructural evolution

The contribution of intense plastic deformation and high-temperature exposure within the stirred zone during FSW/FSP results in recrystallization and development of kết cấu within the stirred zone [7,8,10,15,41,62,63,75-91] and precipitate dissolution and sự tăng trưởng within and around the stirred zone [8,10,41,62,63]. Based on microstructural characterization of grains and precipitates, three distinct zones, stirred (mắt điểm hàn) zone, thermo-mechanically affected zone (TMAZ), and heat-affected zone (HAZ), have been identified as shown in Fig. 17. The microstructural changes in various zones

……

Fig. 17. A typical macrograph showing various microstructural zones in FSP 7075Al-T651 (standard threaded pin, 400 rpm and 51 mm/min).

have significant effect on sau khi hàn mechanical properties. Therefore, the microstructural evolution during FSW/FSP has been studied by a number of investigators.

4.1. Mắt điểm hàn zone

Intense plastic deformation and frictional heating during FSW/FSP result in generation of a recrystallized fine-grained microstructure within stirred zone. This region is usually referred to as mắt

điểm hàn zone (or weld mắt điểm hàn) or dynamically recrystallized zone (DXZ). Under some FSW/FSP conditions, onion ring structure was observed in the mắt điểm hàn zone (Figs. 17 and 18b). In the interior of the recrystallized grains, usually there is low dislocation density [4,5]. However, some investigators reported that the small recrystallized grains of the mắt điểm hàn zone contain high density of sub-boundaries [61], subgrains [75], and dislocations [92]. The interface between the recrystallized mắt điểm hàn zone and the parent metal is relatively diffuse on the retreating side of the tool, but quite sharp on the advancing side of the tool [93].

4.1.1. Shape of mắt điểm hàn zone

Depending on processing parameter, tool geometry, temperature of workpiece, and thermal conductivity of the material, various shapes of mắt điểm hàn zone have been observed. Basically, mắt điểm hàn zone can be classified into two types, basin-shaped mắt điểm hàn that widens near the upper surface and elliptical mắt điểm hàn. Sato et al. [61] reported the formation of basin-shaped mắt điểm hàn on friction stir welding of 6063Al-T5 plate. They suggested that the upper surface experiences extreme deformation and frictional heating by contact with a cylindrical-tool shoulder during FSW, thereby resulting in generation of basin-shaped mắt điểm hàn zone. On the other hand, Rhodes et al. [4] and Mahoney et al. [41] reported elliptical mắt điểm hàn zone in the weld of 7075Al-T651.

Recently, an investigation was conducted on the effect of FSP parameter on the microstructure and properties of cast A356 [94]. The results indicated that lower tool rotation rate of 300-500 rpm resulted in generation of basin-shaped mắt điểm hàn zone, whereas elliptical mắt điểm hàn zone was observed by FSP at higher tool rotation of >700 rpm (Fig. 18). This indicates that with same tool geometry, different mắt điểm hàn shapes can be produced by changing processing parameters.

Reynolds [29] investigated the relationship between mắt điểm hàn size and pin size. It was reported that the mắt điểm hàn zone was slightly larger than the pin diameter, except at the bottom of the weld where the pin tapered to a hemispherical termination (Fig. 19). Further, it was revealed that as the pin diameter increases, the mắt điểm hàn acquired a more rounded shape with a maximum diameter in the middle of the weld.

4.1.2. Grain size

It is well accepted that the dynamic recrystallization during FSW/FSP results in generation of fine and equiaxed grains in the mắt điểm hàn zone [7,8,10,15,41,62,63,75-91]. FSW/FSP parameters, tool geometry, composition of workpiece, temperature of the workpiece, vertical pressure, and active cooling exert significant influence on the size of the recrystallized grains in the FSW/FSP materials.
……

Fig. 18. Effect of processing parameter on mắt điểm hàn shape in FSP A356: (a) 300 rpm, 51 mm/min and (b) 900 rpm, 203 mm/ min (standard threaded pin) [94].

Tables 2 and 3 give a summary of the grain size values for various aluminum alloys under different FSW/FSP conditions. The tool geometry was not identified in a number of studies. While the typical recrystallized grain size in the FSW/FSP aluminum alloys is in the micron range (Table 2), ultrafine-grained (UFG) microstructures (average grain size <1 mm) have been achieved by using external cooling or special tool geometries (Table 3).

Table 2
A summary of grain size in mắt điểm hàn zone of FSW/FSP aluminum alloys

Table 3
A summary of ultrafine-grained microstructures produced via FSW/FSP in aluminum alloys
……..

(mm) Tool geometry Special cooling Rotation Traverse rate (rpm) speed
……..

Benavides et al. [7] investigated the effect of the workpiece temperature on the grain size of FSW 2024Al. They [7] reported that decreasing the starting temperature of workpiece from 30 to —30 °C with liquid nitrogen cooling resulted in a decrease in the peak temperature from 330 to 140 °C at a location 10 mm away from the đường trục hàn, thereby leading to a reduction in the grain size from 10 to 0.8 mm in FSW 2024Al. Following the same approach, Su et al. [95] prepared bulk nanostructured 7075Al with an average grain size of ~100 nm via FSP, using a mixture of water, methanol and dry ice for cooling the plate rapidly behind the tool. On the other hand, Kwon et al. [63,90,91] adopted a cone¬shaped pin with a sharpened tip to reduce the amount of frictional heat generated during FSP of 1050Al. A peak temperature of only 190 °C was recorded in the FSP zone at a tool rotation rate of 560 rpm and a traverse speed of 155 mm/min, which resulted in grain size of 0.5 mm. Similarly, Charit and Mishra [96] reported that a grain size of 0.68 mm was produced, by using a small diameter tool with normal threaded pin, in FSP of cast Al-Zn-Mg-Sc at a tool rotation rate of 400 rpm and a traverse speed of 25.4 mm/min. These observations are consistent with the general principles for recrystalliza¬tion [97] where the recrystallized grain size decreases with decreasing annealing temperature.

More recently, Li et al. [10], Ma et al. [15], Sato et al. [67], and Kwon et al. [63,90,91] studied the influence of processing parameter on the microstructure of

FSW/FSP aluminum alloys. It was noted that the recrystallized grain size can be reduced by decreasing the tool rotation rate at a constant tool traverse speed [10,63,67,90,91] or decreasing the ratio of tool rotation rate/traverse speed [15]. For example, Kwon et al. [63,90,91] reported that FSP resulted in generation of the grain size of ~0.5,1-2, and 3-4 mm in 1050Al at tool rotation rate of 560, 980, 1840 rpm, respectively, at a constant traverse speed of 155 mm/min. Similarly, Sato et al. [67] reported the grain size of 5.9, 9.2, and 17.8 mm in FSW 6063Al at tool rotation rate of 800, 1220, 2450 rpm, respectively, at a constant traverse speed of

……..

Fig. 20. Effect of FSP parameters on mắt điểm hàn grain size in FSP 7075Al-T7651 at processing parameter of: (a) 350 rpm, 152 mm/min and (b) 400 rpm, 102 mm/min [15].

360 mm/min. Fig. 20 shows the optical micrographs of FSP 7075A1-T651 processed by using two different processing parameter combinations. Decreasing the ratio of tool rotation rate/traverse speed from 400 rpm/102 mm/min to 350 rpm/152 mm/min resulted in a decrease in the recrys¬tallized grain size from 7.5 to 3.8 mm. FSW/FSP at higher tool rotation rate or higher ratio of tool rotation rate/traverse speed results in an increase in both degree of deformation and peak temperature of thermal cycle. The increase in the degree of deformation during FSW/FSP results in a reduction in the recrystallized grain size according to the general principles for recrystallization [97].

On the other hand, the increase in peak temperature of FSW/FSP thermal cycle leads to generation of coarse recrystallized grains, and also results in remarkable grain growth. A recent investigation on FSP 7050Al has revealed that the initial size of newly recrystallized grains is on the order of 25-100 nm [98]. When heated for 1-4 min at 350-450 °C, these grains grow to 2-5 mm, a size equivalent to that

found in FSP aluminum alloys [98]. Therefore, the variation of recrystallized grain size with tool rotation rate or traverse speed in FSW/FSP aluminum alloys depends on which factor is dominant.

The investigations on FSP 1050Al and 7075Al-T651 appear to indicate that the peak temperature of FSW/FSP thermal cycle is the dominant factor in determining the recrys¬tallized grain size. Thus, the recrystallized grain size in the FSW/FSP aluminum alloys generally increases with increasing the tool rotation rate or the ratio of tool rotation rate/traverse speed. Fig. 21 shows the variation of grain size with pseudo-heat index in 2024Al and 7075Al [99]. It shows that there is an optimum combination of tool rotation rate and traverse speed for generating the finest grain size in a specific aluminum alloy with same tool geometry and temperature of the workpiece.

The grain size within the weld zone tends to increase near the top of the weld zone and it decreases with distance on either side of the weld-zone centerline, and this corresponds roughly to temperature variation within the weld zone [8,10,41]. For example, Mahoney et al. [100] reported a variation in grain size from the bottom to the top as well as from the advancing to the retreating side in a 6.35 mm- thick FSP 7050Al. Fig. 22 shows the distribution of the grain sizes in different locations of the mắt điểm hàn zone of FSP 7050Al [100]. The average grain size ranges from 3.2 mm at the bottom to 5.3 mm at the top and 3.5 mm from the retreating side to 5.1 mm on the advancing side. Similarly, in a 25.4 mm thick plate of FSW 2519Al, it was found that the average grain sizes were 12, 8 and 2 mm, respectively, in
……..

Fig. 22. Grain size distribution in various locations of 7050Al weld mắt điểm hàn [100].
the top, middle, and bottom region of the weld mắt điểm hàn [89]. Such variation in grain size from

bottom to top of the weld mắt điểm hàn is believed to be associated with difference in temperature profile and heat dissipation in the mắt điểm hàn zone. Because the bottom of workpieces is in contact with the backing plate, the peak temperature is lower and the thermal cycle is shorter compared to the mắt điểm hàn top. The combination of lower temperature and shorter excursion time at the mắt điểm hàn bottom effectively retards the grain growth and results in smaller recrystallized grains. It is evident that with increasing plate thickness, the temperature difference between bottom and top of the weld mắt điểm hàn increases, resulting in increased difference in grain size.

4.1.3. Recrystallization mechanisms

Several mechanisms have been proposed for dynamic recrystallization process in aluminum alloys, such as discontinuous dynamic recrystallization (DDRX), continuous dynamic recrystalliza¬tion (CDRX), and geometric dynamic recrystallization (GDRX) [97,101-106]. Aluminum and its alloys normally do not undergo DDRX because of their high rate of recovery due to aluminum ’ s high stacking-fault energy [101,105]. However, particle-simulated nucleation of DDRX is observed in alloys with large (>0.6 mm) secondary phases [101-106]. The DDRX is characterized by nucleation of new grains at old high-angle boundaries and gross grain boundary migration [97]. On the other hand, CDRX has been widely studied in commercial superplastic aluminum alloys [107-111] and two-phase stainless steels [112-114]. Several mechanisms of CDRX have been proposed whereby subgrains rotate and achieve a high misorientation angle with little boundary migration. For example, mechanisms include subgrain growth [107], lattice rotation associated with sliding [108,111], and lattice rotation associated with slip [114].

As for dynamic nucleation process in the mắt điểm hàn zone of FSW aluminum alloys, CDRX [6,75,84], DDRX [67,95,98], GDRX [69,115], and DRX in the adiabatic shear bands [116] have been proposed to be possible mechanisms. Jata and Semiatin [6] were the first to propose CDRX as operative dynamic nucleation mechanism during FSW. They suggested

that low-angle boundaries in the parent metal are replaced by high-angle boundaries in the mắt điểm hàn zone by means of a continuous rotation of the original low-angle boundaries during FSW. In their model, dislocation glide gives rise to a gradual relative rotation of adjacent subgrains. Similarly, Heinz and Skrotzki [75] also proposed that CDRX is operative during FSW/FSP. In this case, strain induces progressive rotation of subgrains with little boundary migration. The subgrains rotation process gradually transforms the boundaries to high-angle grain boundaries.

[redacted]

However, it is important to point out that many of the recrystallized grains in the mắt điểm hàn zone are finer than the original subgrain size. Thus, it is unlikely that the recrystallized grains in the mắt điểm hàn zone result from the rotation of original elongated subgrains in the base metal. Recently, Su et al. [84] conducted a detailed microstructural investigation of FSW 7050Al-T651. Based on microstructural observations, they suggested that the dynamic recrystallization in the mắt điểm hàn zone can be considered a CDRX on the basis of dynamic recovery. Subgrain growth associated with absorption of dislocation into the boundaries is the CDRX mechanism. Repeated absorption of dislocations into subgrain boundaries is the dominant mechanism for increasing the misorientation between adjacent subgrains during the CDRX.

[redacted]

Alternatively, DDRX has been recently proposed as an operative mechanism for dynamic nucleation process in FSW/FSP aluminum alloys based on recent experimental observations[95.98] . Su et al. [95] reported generation of recrystallized grains of ~0.1 mm in a FSP 7075Al by means of rapid cooling behind the tool. Similarly, Rhodes et al. [98] obtained recrystallized grains of 25-100 nm in FSP 7050Al-T76 by using ‘‘plunge and extract ’ ’ technique and rapid cooling. These recrystallized grains were significantly smaller than the pre-existing subgrains in the parent alloy, and identified as non-equilibrium in nature, predominantly high-angled,

[redacted]

relatively dislocation-free [95.98] . Su et al. [95] and Rhodes et al. [98] proposed that DDRX mechanism is responsible for the nanostructure evolution.

The fact that recrystallized grains in the mắt điểm hàn zone of FSW/FSP aluminum alloys are significantly smaller than the pre-existing subgrains in the parent alloy strongly suggests that DDRX is the operative mechanism for recrystallization during FSW/FSP of aluminum alloys.

4.1.4. Precipitate dissolution and sự tăng trưởng

As presented in Section 3.2, FSW/FSP results in the temperature increase up to 400-550 °C within the mắt điểm hàn zone due to friction between tool and workpieces and plastic deformation around rotating pin [4,5,41,60-63,67,68]. At such a high temperature precipitates in aluminum alloys can coarsen or dissolve into aluminum matrix depending on alloy type and maximum temperature.

Liu et al. [5] investigated the micmstn.icri.iie of a friction stir welded 6061Al-T6. They reported that the homogenously distributed precipitates are generally smaller in the workpiece than in the mắt điểm hàn zone. However, there were far fewer large precipitates in the mắt điểm hàn zone than in the base material. This implies the occurrence of both dissolution and sự tăng trưởng of precipitates during FSW. Recently, Sato et al. [61] examined the microstructural evolution of a 6063Al-T5 during FSW using TEM. They did not observe precipitates within the mắt điểm hàn zone, indicating that all the precipitates were dissolved into aluminum matrix during FSW. More recently, Heinz and Skrotzki [75] also reported complete dissolution of the precipitates in FSW 6013Al-T6 and 6013Al-T4 with a tool rotation rate of 1400 rpm and a traverse speed of 400-450 mm/min. Similarly, in FSW 7XXX aluminum alloys (7075Al-T7451), Jata et al. [92] also observed the absence of strengthening precipitates in the mắt

điểm hàn zone, indicating complete dissolution of the precipitates. The overall response includes a combination of dissolution, sự tăng trưởng and reprecipitation of strengthening precipitates during FSW/FSP.

4.1.5. Kết cấu

Kết cấu influences a variety of properties, including strength, ductility, formability and corrosion resistance. As mentioned earlier, the FSW material consists of distinct microstructural zones, i.e., mắt điểm hàn, TMAZ, HAZ and base material. Each zone has different thermo-mechanical history. What is even more complicated for FSW is that the mắt điểm hàn region consists of sub-domains. For example, the top layer undergoes deformation by shoulder after the pin has passed through. In addition, depending on the tool rotation rate and traverse speed, the mắt điểm hàn region can contain ring pattern or other microstructural variations. A few kết cấu studies of FSW aluminum alloys have been reported [117¬120]. In the last decade, the use of microt.ext.ure using orientation imaging microscopy (OIM) has proved to be a very valuable tool in not only obtaining the kết cấu information, but also establish the grain boundary misorientation distribution data from same set of experiments.

Sato et al. [118] and Field et al. [119] have reported detailed kết cấu analysis through the FSW welds. The overall plots of grain boundary misorientation distribution showed that the mắt điểm hàn region predominantly consisted of high-angle grain boundaries. However, the microkết cấu results showed complex kết cấu pattern. Sato et al. [118] noted that the Goss orientation in the parent 6063Al changed to shear kết cấu component with two types of orientation in the center of the mắt điểm hàn. The pole figures were examined for the surface and center regions on both sides of the center line, i.e., on the advancing and retreating sides. An important

observation that emerged, by comparing pole figures at 2.5, 3.3, and 4 mm away on both sides from the center, was that the đường trục hàn roughly contained {1 10} (0 01) and {114} (2 21) shear kết cấu components.

However, these components were rotated around the 'normal direction', the direction of the axis of pin. Both these components were also observed by Field et al. [119], including the rotational aspect of the kết cấu component from the advancing side to the retreating side. During FSW, the material undergoes intense shearing and dynamic recrystallization concurrently. One of the key issues to understand is how nucleation of new grains and continuous deformation influence the final kết cấu results. In addition, it is important to separate out the effect of final deformation by shoulder through the forging action after the pin has passed. The deformation under shoulder is likely to influence the final kết cấu significantly. It adds a shear deformation component at lower temperature to the recrystallized volume processed by the pin.

4.2. Thermo-mechanically affected zone

Unique to the FSW/FSP process is the creation of a transition zone—thermo-mechanically affected zone (TMAZ) between the parent material and the mắt điểm hàn zone [4,15,41], as shown in Fig. 17. The TMAZ experiences both temperature and deformation during FSW/FSP. A typical micrograph of TMAZ is shown in Fig. 23. The TMAZ is characterized by a highly deformed structure. The parent metal elongated grains were deformed in an upward flowing pattern around the mắt điểm hàn zone. Although the TMAZ underwent plastic deformation, recrystallization did not occur in this zone due to insufficient deformation strain. However, dissolution of some precipitates was observed in the TMAZ, as shown in Fig. 24c and d, due to high-temperature exposure during FSW/FSP [61,84]. The extent of dissolution, of course, depends on the thermal cycle experienced by TMAZ. Furthermore, it was revealed that the grains in the TMAZ usually contain a high density of sub-boundaries [61].

……

Fig. 23. Microstructure of thermo-mechanically affected zone in FSP 7075Al [15].

4.3. Heat-affected zone

Beyond the TMAZ there is a heat-affected zone (HAZ). This zone experiences a thermal cycle, but does not undergo any plastic deformation (Fig. 17). Mahoney et al. [61] defined the HAZ as a zone experiencing a temperature rise above 250 °C for a heat-treatable aluminum alloy. The HAZ retains

……..

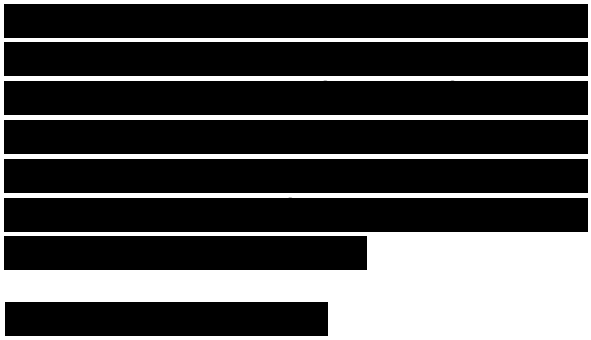

Fig. 24. Precipitate microstructures in the grain interior and along grain boundaries in: (a) base metal, (b) HAZ, (c) TMAZ near HAZ, and (d) TMAZ near mắt điểm hàn zone (FSW 7050Al-T651, tool rotation rate: 350 rpm, traverse speed: 15 mm/min) (after Su et al. [84]).

the same grain structure as the parent material. However, the thermal exposure above 250 °C exerts a significant effect on the precipitate structure.

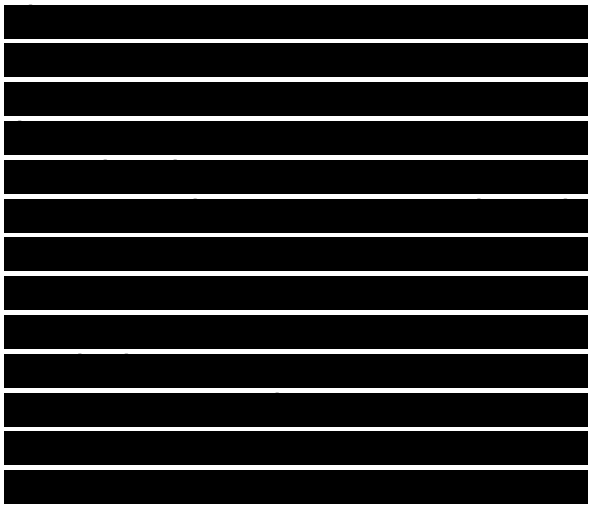

Recently, Jata et al. [92] investigated the effect of friction stir welding on microstructure of 7050Al-T7451 aluminum alloy. They reported that while FSW process has relatively little effect on the size of the subgrains in the HAZ, it results in sự tăng trưởng of the strengthening precipitates and the precipitate-free zone (PFZ) increases by a factor of 5. Similar observation was also made by Su et al. [84] in a detailed TEM examination on FSW 7050Al-T651 (Fig. 24b). The sự tăng trưởng of precipitates and widening of PFZs is evident. Similarly, Heinz and Skrotzki [75] also observed significant sự tăng trưởng of the precipitates in the HAZ of FSW 6013Al.

5

. Properties

5.1. Residual stress

During fusion welding, complex thermal and mechanical stresses develop in the weld and surrounding region due to the localized application of heat and accompanying constraint. Following fusion welding, residual stresses commonly approach the yield strength of the base material. It is generally believed that residual stresses are low in friction stir welds due to low temperature solid-state process of FSW.

However, compared to more compliant clamps used for fixing the parts in conventional welding processes, the rigid clamping used in FSW exerts a much higher restraint on the welded plates. These restraints impede the contraction of the weld mắt điểm hàn and heat-affected zone during cooling in both longitudinal and transverse directions, thereby resulting in generation of longitudinal and transverse stresses. The existence of high value of residual stress exerts a significant effect on the sau khi hàn mechanical properties, particularly the fatigue properties. Therefore, it is of practical importance to investigate the residual stress distribution in the FSW welds.

James and Mahoney [93] measured residual stress in the FSW 7050Al-T7451, C458 Al-Li alloy, and 2219Al by means of Tia X diffraction sin2 C method. Typical results obtained in FSW 7050Al- T7451 by pinhole Tia X beam (1 mm) are tabulated in Table 4. This investigation revealed following findings. First, the residual stresses in all the FSW welds were quite low compared to those generated during fusion welding. Second, at the transition between the fully recrystallized and partially recrystallized regions, the residual stress was higher than that observed in other regions of the weld. Third, generally, longitudinal (parallel to welding direction) residual stresses were tensile and transverse (normal to welding direction) residual stresses were compressive. The low residual stress

Table 4

Residual stress measurement (MPa) in FSW 7050Al-T6541 weld by pinhole beam Tia X (after James and Mahoney [93])
Location
Distance from weld centreline (mm)
Longitudinal
Transverse

Retreating side
Advancing side
Retreating side
Advancing side
…….

Distance from Đường trục hàn, mm
Fig. 25. Longitudinal residual stress distribution in FSW 6013A1-T4 welds determined by different measurement methods (tool rotation rate: 2500 rpm, traverse speed: 1000 mm/min, tool shoulder diameter: 15 mm) (after Donne et al. [121]).

in the FSW welds was attributed to the lower heat input during FSW and recrystallization accommodation of stresses [93].

Recently, Donne et al. [121] measured residual stress distribution on FSW 2024Al-T3 and 6013Al-T6 welds by using the cut compliance technique, Tia X diffraction, neutron diffraction and high-energy synchrotron radiation. Six important observations can be made from their study. First, the experimental results obtained by these measurement techniques were in good qualitative and quantitative agreement. Second, the longitudinal residual stresses were always higher than the transverse ones, independent

on pin diameter, tool rotation rate and traverse speed.

Third, both longitudinal and transverse residual stresses exhibited an ‘‘M’’-like distribution across the weld. A typical longitudinal residual stress distribution is shown in Fig. 25. Fig. 25 reveals that maximum tensile residual stresses were located ~10 mm away from the đường trục hàn, i.e., the HAZ. Small compressive residual stresses were detected in the parent metal adjacent to the HAZ and the weld seam. Fourth, residual stress distribution across the welds was similar at the top and root sides of the welds. Fifth, large-diameter tool widened the M-shaped residual stress distribution.

With decreasing welding speed and tool rotation rate, the magnitude of the tensile residual stresses decreased. Sixth, in the case of the small samples of 30 mm x 80 mm and 60 mm x 80 mm, the maximum longitudinal tensile residual stresses were in the range of 30-60% of weld material yield strength and 20-50% of base material yield strength. Clearly, the residual stress values in the FSW welds are remarkably lower than those in the fusion welds. However, Wang et al. [122] reported that larger values of residual stress may be present in larger samples of 200 mm x 200 mm.

More recently, Peel et al. [123] investigated the residual stress distribution on FSW 5083Al using synchrotron Tia X diffraction. Following observations can be made from their investigation. First, while longitudinal residual stress exhibited a ‘‘M’’-like distribution across the weld similar to the results of Donne et al. [121], transverse residual stresses exhibited a peak at the đường trục hàn.

Second, the mắt điểm hàn zone was in tension in both longitudinal and transverse directions. Third, peak tensile residual stress was observed at ~10 mm from the đường trục hàn, a distance corresponding to the edge of the tool shoulder. Fourth, longitudinal residual stress increased with increasing tool traverse speed, whereas transverse residual stresses did not exhibit evident dependence on the traverse speed.

Fifth, a mild asymmetry in longitudinal residual stress profile was observed within the mắt điểm hàn zone with the stresses being ~10% higher on the advancing side. Sixth, similar to the results of Donne et al. [121],

……..

Fig. 26. Average, through thickness, longitudinal and traverse residual stress distribution as a function of distance from the đường trục hàn in FSW 204L stainless steel (tool traverse speed: 102 mm/min) (after Reynolds et al. [124]).

maximum residual stresses in longitudinal direction (40-60 MPa) were higher than those in transverse direction (20-40 MPa).

Clearly, maximum residual stresses observed in various friction stir welds of aluminum alloys were below 100 MPa [121-123]. The residual stress magnitudes are significantly lower than those observed in fusion welding, and also significantly lower than yield stress of these aluminum alloys. This results in a significant reduction in the distortion of FSW components and an improvement in mechanical properties.

On the other hand, Reynolds et al. [124] measured residual stress of 304L stainless steel FSW welds by neutron diffraction. Average, through thickness, longitudinal and transverse residual stresses are presented in Fig. 26 as a function of distance from the đường trục hàn. Fig. 26 revealed the following observations. First, the residual stress patterns observed for FSW are typical of most welding processes such as fusion welding, namely, high value of longitudinal tensile residual stress and very low transverse residual stress. Second, the maximum values of longitudinal residual stress were close to the base metal yield stress, and therefore similar in magnitude to those produced by fusion welding processes in austenitic stainless steels [125].

Third, increasing tool rotation rate from 300 to 500 rpm at a constant tool traverse speed of 102 mm/min did not exert marked effect on the residual stress distribution apart from slightly widening the range of high values of residual stress. Further, Reynolds et al. [124] reported that the longitudinal residual stress varied only slightly with depth, whereas the transverse stress varied significantly through the thickness. The sign of the transverse residual stress near the đường trục hàn was in general positive at the crown and negative at the root. This was attributed to rapid cooling experienced by the weld root due to the intimate contact between the weld root side and the backing plate. Clearly, the distribution and magnitude of residual stress in friction stir welds are different for aluminum alloy and steel. This is likely to be related to the temperature dependence of the yield strength and the influence of final deformation by the trailing edge of the tool shoulder.

5.2. Hardness

Aluminum alloys are classified into heat-treatable (precipitation-hardenable) alloys and non¬heat-treatable (solid-solution-hardened) alloys. A number of investigations demonstrated that the change in hardness in the friction stir welds is different for precipitation-hardened and solid-solution-

……

Fig. 27. Typical hardness curve across the weld of FSW 6063A1-T5 (after Sato et al. [61]).

hardened aluminum alloys. FSW creates a softened region around the đường trục hàn in a number of precipitation-hardened aluminum alloys [5,7,10,61,126,127]. It was suggested that such a softening is caused by sự tăng trưởng and dissolution of strengthening precipitates during the thermal cycle of the FSW [5,7,10,61,126,127]. Sato et al. [61] have examined the hardness profiles associated with the microstructure in an FSW 6063Al-T5. They reported that hardness profile was strongly affected by precipitate distribution rather than grain size in the weld. A typical hardness curve across the weld of

FSW 6063Al-T5 is shown in Fig. 27. The average hardness of the solution-treated base material is also included in Fig. 27 for comparison. Clearly, significant softening was produced throughout the weld zone, compared to the base material in T5 condition. Further, Fig. 27 shows that the lowest hardness does not lie in the center part of the weld zone, but is 10 mm away from the đường trục hàn. Sato et al. [61] labeled the hardness curves by BM (the same hardness region as the base material), LOW (the

……..

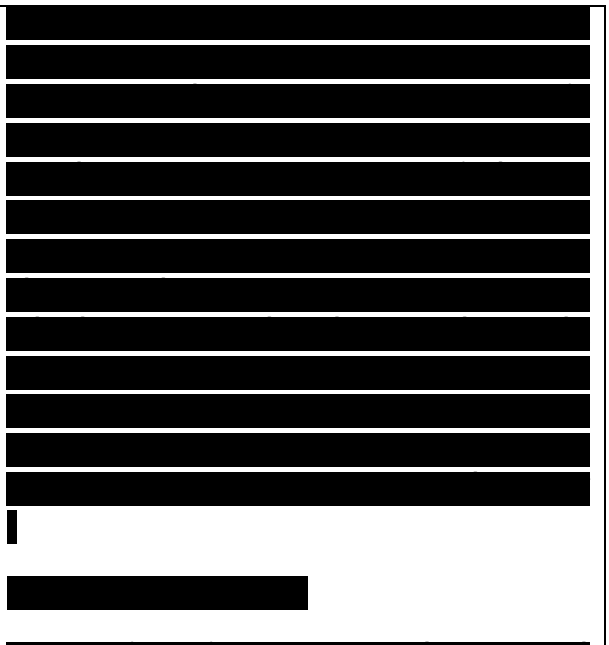

Fig. 28. TEM micrographs showing precipitate distribution in various microstructural zones in FSW 6063Al-T5 (after Sato et al. [61]).

region of lower hardness than base material), MIN (the minimum-hardness region), and SOF (the softened region) (Fig. 27), and examined the micmstn.icri.ii c of these four regions. As shown in Fig. 28, two kinds of precipitates are observed in the BM, LOW, and MIN regions; needle-shaped precipitates of about 40 nm in length, which are partially or completely coherent with the matrix, and rod-shaped precipitates approximately 200 nm in length, which have low coherency with the matrix. The mechanical properties of 6063Al depend mainly on the density of needle-shaped precipitates and only slightly on the density of rod-shaped precipitates [128,129].

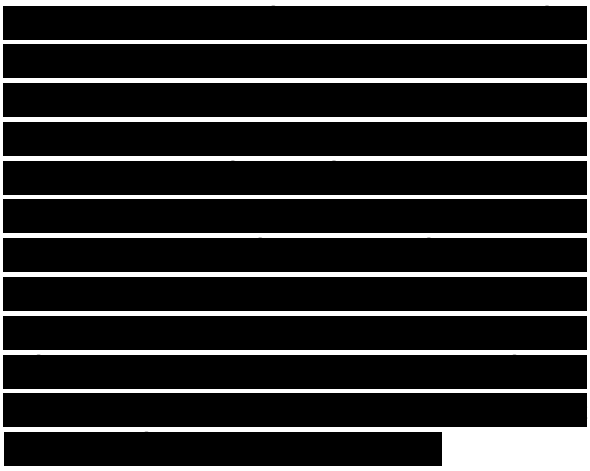

Sato et al. [61] reported that the microstructure (type, size and distribution of precipitates) in the BM region was basically the same as that in the base material (Fig. 28a), which explains the same hardness in the BM region and the base material. In the LOW region, the density of needle-shaped precipitates was substantially reduced, whereas the density of rod-shaped precipitates was increased (Fig. 28b). This resulted in a reduction in hardness of the LOW region. For the MIN region, only low density of rod-shaped precipitates remained (Fig. 28c). Thus, not only the hardening effect of needle-shaped

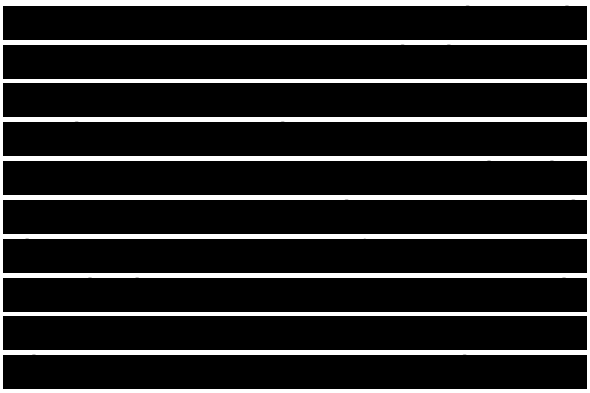

disappeared completely, but also solid-solution-hardening effect of solutes was reduced due to the existence of rod-shaped precipitates, which leads to the minimum hardness in the MIN region. In the SOF region, no precipitates were detected due to complete dissolution of the precipitates (Fig. 28d). Sato et al. [61] suggested that the somewhat higher hardness in the SOF region than in the base material was explained by the smaller grain size and higher density of sub-boundaries.

For the solid-solution-hardened aluminum alloys, generally, FSW does not result in softening in the welds [9,78,130]. For 5083Al-0 containing small particles, the hardness profile was roughly uniform in the weld [78,130], whereas for 1080Al-0 without any second-phase particles, the hardness in the mắt điểm hàn zone was slightly higher than that in the base material, and the maximum hardness was located in the TMAZ [78]. Microstructural factors governing the hardness in the FSW welds of the solid-solution-hardened aluminum alloys were suggested by various investigators [9,78,130]. In an investigation on the microstructure and properties of FSW 5083Al-0, Svesson et al. [130] reported that the mắt điểm hàn zone had fine equiaxed grains with a lower density of large particles (1-10 |mm) and a higher density of small particles (0.1-1 mm). They suggested that the hardness profile mainly depended on dislocation density, because the dominant hardening mechan¬ism for 5083Al is strain hardening. On the other hand, Sato et al. [78] reported that FSW created the fine recrystallized grains in the mắt điểm hàn zone and recovered grains in the TMAZ in 5083Al-O with the mắt điểm hàn zone and the TMAZ having slightly higher dislocation densities than the base material. Both small and large Al6(Mn,Fe) particles were detected in the mắt điểm hàn zone and the base material. They concluded that the hardness profile could not be explained by the Hall-Petch relationship, but rather by Orowan strengthening, namely, the hardness profile in the FSW 5083Al was dominantly governed by the dispersion strengthening due to distribution of small particles. In this case, the interparticle spacing is likely to be much lower than the grain size. For the FSW 1080Al-O, Sato et al. [78] reported that the mắt điểm hàn zone consisted of

recrystallized grains with a low density of dislocations, while the TMAZ had recovered grains with a subgrain structure. The overall behavior is governed by the relative strengthening contributions from grain boundaries, particles and substructure.	[redacted]

5.3. Mechanical properties

FSW/FSP results in significant microstructural evolution within and around the stirred zone, i.e., mắt điểm hàn zone, TMAZ, and HAZ. This leads to substantial change in sau khi hàn mechanical properties. In the following sections, typical mechanical properties, such as strength, ductility, fatigue, and fracture toughness are briefly reviewed.

Table 5
Longitudinal tensile properties of weld mắt điểm hàn in friction stir welded 7075Al-T651 at room temperature (after Mahoney et al. [41])

.....

Sau khi hàn age treatment 496

5.3.1. Strength and ductility

Mahoney et al. [41] investigated the effect of FSW on room-temperature tensile properties of 7075Al-T651. Tensile specimens were machined from the mắt điểm hàn zone in two directions, parallel (longitudinal) and normal (transverse) to the weld. Longitudinal tensile specimens contained only fully recrystallized grains from the mắt điểm hàn zone, whereas transverse tensile specimens contained microstructures from all four zones, i.e., parent material, HAZ, TMAZ, and mắt điểm hàn zone. Table 5 summarizes the longitudinal tensile properties of mắt điểm hàn zone. As-welded samples show a reduction in yield and ultimate strengths in the weld mắt điểm hàn, while elongation was unaffected. Mahoney et al. [41] attributed the reduced strength to the reduction in pre-existing dislocations and the elimination of the very fine hardening precipitates [4].

In order to recover the lost tensile strength of the mắt điểm hàn zone, Mahoney et al. [41] conducted a sau khi hàn aging treatment (121 °C/24h) on the FSW sample. As shown in Table 5, the aging treatment resulted in recovery of a large portion of the yield

strength in the mắt điểm hàn, but at the expense of ultimate strength and in particularly ductility. The increase in the yield strength of sau khi hàn samples was attributed to the increase in the volume fraction of fine hardening precipitates, whereas the reduction in the ductility was accounted for by both the increase in the hardening precipitates and the development of precipitate-free zones (PFZs) at grain boundaries [41]. The tensile properties in transverse orientation of FSW 7075Al-T651 are summarized in Table 6. Compared to unwelded parent metal, samples tested in transverse direction show a significant reduction in both strength and ductility. Furthermore, the strength and ductility observed in transverse orientation are also substantially less than those in longitudinal orientation. The sau khi hàn aging treatment did not restore any of the strength to the as-welded condition and further reduced ductility. In both as-welded and aged condition, failures occurred as shear fracture in the HAZ. As reported before, the tensile specimens in the transverse orientation cover four different microstructures, i.e., parent material, HAZ, TMAZ, and mắt điểm hàn zone. The observed ductility is an average strain over the gage length including various zones. The different zones have different resistances to deformation due to differences in grain size and precipitate size and distribution as discussed in Section 4. The HAZ has the lowest strength due to significantly coarsened precipitates and the development of the FPZs. Thus, during tension, strain occurs mainly in the HAZ. As shown in Fig. 29, the low-strength HAZ locally elongated to high levels of strain (12-14%), eventually resulting in necking and fracture, whereas the mắt điểm hàn zone experiences only 2-5% strain. Therefore, fracture always occurred in the HAZ, resulting in a low strength and ductility along transverse orientation of the weld.

Table 6
Room-temperature tensile properties in transverse orientation of friction stir welded 7075Al-T651 (after

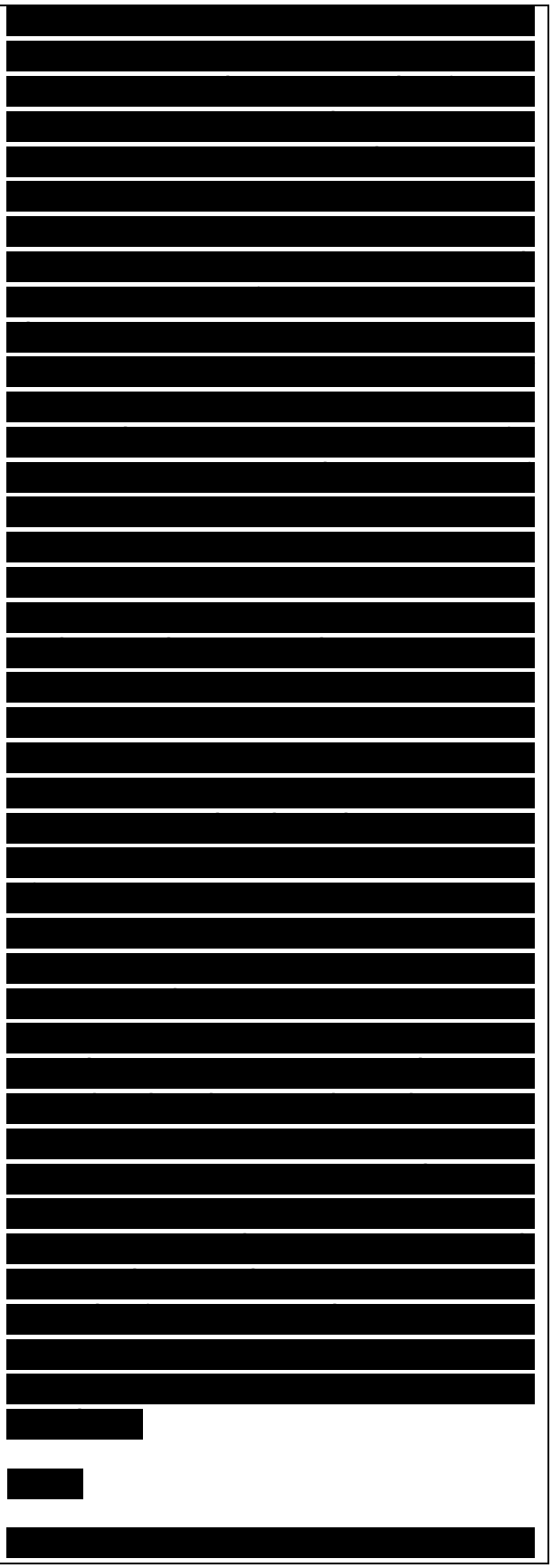

Mahoney et al. [41])
……

Fig. 29. Tensile strain distribution within the HAZs and weld mắt điểm hàn of FSW 7075A1-T651 weld (after Mahoney et al. [41]).

Recently, Sato et al. [78] investigated the transverse tensile properties of the friction stir weld of 6063-T5 aluminum. In order to reveal the effect of sau khi hàn treatment on the weld properties, sau khi hàn aging (175 °C/12 h) and sau khi hàn solution heat treatment and aging (SHTA, 530 °C/ 1 h + 175 °C/12 h) were conducted on the welds. Fig. 30 shows the tensile properties of the base material, the weld, aged weld, and the SHTA weld. Fig. 30 reveals that the strengths and elongation are lowest in the as-welded weld. The aged weld has slightly higher strengths than the base material with

Fig. 30. Tensile properties of base metal, as-welded weld, aged weld, and SHTA weld for 6063Al-T5 (after Sato et al. [78]).

Table 7
Room-temperature tensile properties of base material and welded joints in both longitudinal (L) and transverse (T) orientations of FSW 2024Al-T3 plates of 4 and 1.6 mm thickness (after Biallas et al. [40])
……

concurrently improved ductility. The SHTA increases the strengths of the weld to above those of the base material with almost completely restored ductility. Sato et al. [78] reported that the strain of the as-welded weld was localized in a region 5-6 mm from the đường trục hàn, i.e. the minimum-hardness region (MIN) as discussed previously in Section 5.2, resulting in final fracture with low strength and ductility. Sau khi hàn aging leads to reprecipitation of the needle-shaped precipitates in the weld, resulting in a shift in the minimum hardness from the original

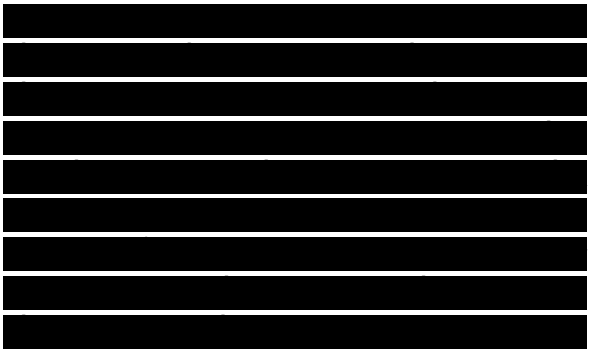

MIN to low hardness (LOW) region. This is because the high density of large b' precipitates in the LOW region of as-welded weld consume large amount of the solutes, thereby reduced the density of the needle-shaped precipitates during the sau khi hàn aging. Thus, fracture occurred in a region 7-8 mm from the đường trục hàn, i.e., original LOW. On the other hand, the solution heat-treatment produces a supersaturated solid solution throughout the specimen, and the subsequent aging leads to the homogenous reprecipitation of the needle-shaped precipitates. This results in increased strength and homogeneous distribution of strain throughout the weld. In this case, the fracture occurred in the base material region. Further, fracture locations of all welds were at the retreating side.

Biallas et al. [40] studied the effect of FSW parameters on the tensile properties of FSW 2024Al-T4. The tensile properties are summarized in Table 7. It is evident from Table 7 that for a constant ratio of tool traverse speed/rotation rate, both yield and ultimate strengths increase with increasing tool rotation rate and ductility is also improved. Furthermore, Table 7 reveals that higher strength and joining efficiency were observed in thinner plates than in thicker plates.

Table 8 summarizes the transverse tensile strength of FSW welds and joining efficiency of FSW welds for various aluminum alloys. This table reveals that the joining efficiency of FSW welds ranges from 65 to 96% for heat-treatable aluminum alloys and is 95-119% for non-heat-treatable aluminum alloy 5083Al. The joining efficiency for FSW is significantly higher than that for conventional fusion welding, particularly for heat-treatable aluminum alloys.

It should be emphasized that the strengths obtained in

the transverse tensile test of the FSW weld using large specimens represent the weakest region of the weld and the elongation is an average strain over the gage length including various zones. Although such a tensile test is meaningful for engineering applications, it does not provide an insight into the correlation between the intrinsic tensile properties and localized microstructure. Therefore, it is necessary to utilize a more suitable test technique to establish the intrinsic tensile properties of the weld associated with localized micro¬structure. Recently, two studies were conducted by von Strombeck et al. [135] and Mishra et al. [139] to determine the tensile properties at different locations of the FSW welds using mini tensile specimens. Similar experimental results were reported in these two studies. A typical variation of tensile properties with the position across the weld of FSW 7075Al alloy is shown in Fig. 31. Fig. 31

Table 8
Friction stir weld joint efficiency for various aluminum alloys
…….

shows the following important findings. First, the strength is almost constant in the mắt điểm hàn zone. While the yield strength in the mắt điểm hàn zone is ~80% of the base material, the ultimate strength is close to 100% and the ductility is significantly improved. The combination of comparable ultimate strength and higher ductility was attributed to the fine-grained microstructure in the mắt điểm hàn zone [139]. Second, approaching the mắt điểm hàn/TMAZ transition region, the strength remains similar to the mắt điểm hàn zone, but the ductility starts decreasing toward the baseline. The decrease in ductility as compared to the mắt điểm hàn center can be correlated to the fact that the TMAZ retains the deformed structure. Third, both yield and ultimate

strengths start to drop beyond ±7 mm (TMAZ/HAZ) from the đường trục hàn. The lowest strength, ~60% of base material, was observed in the HAZ (12 mm away from the đường trục hàn on the retreating side). It is surprising that the drop in strength is not accompanied by an increase in ductility. These results provided additional insight to the large-specimen results of Mahoney et al. [41] and Sato et al. [78]. The locally concentrated strain of up to 14% occurred in the HAZ of large- specimen is due to low strength of the HAZ and did not mean that the HAZ has better ductility than other regions. Fourth, the intrinsic strength and ductility of retreating and advancing sides are different. The retreating side has lower strength. This is consistent with the previous observation that fracture always occurred on the retreating side [78].

5.3.2. Fatigue

For many applications, like aerospace structures, transport vehicles, platforms, and bridge constructions, fatigue properties are critical. Therefore, it is important to understand the fatigue characteristics of FSW welds due to potentially wide range of engineering applications of FSW technique. This has led to increasing research interest on evaluating the fatigue behavior of FSW welds, including stress-number of cycles to failure (S-N) behavior [40,89,140-145] and fatigue crack propagation (FCP) behavior [89,92,137,138,146,147].

5.3.2.1. S-N behavior.

In the past few years, several investigations were conducted on the S-N behavior of FSW 6006Al-T5 [140,141], 2024Al-T351 [142], 2024Al-T3 [40], 2024Al-T3, 6013Al- T6, 7475Al-T76 [136], 2219Al-T8751 [145], and 2519Al-T87 [89]. These studies resulted in the following five important observations. First, the fatigue strength of the FSW weld at 107 cycles was lower than that of the base metal, i.e., the FSW welds are susceptible to fatigue crack initiation

…….

Fig. 32. S-N curves of base metal, FSW weld, laser weld and MIG weld for 6005Al-T5 (after Hori et al. [140]).

[40,136,143-146]. Further, Bussu and Irving [147] showed that the transverse FSW specimens had lower fatigue strength than the longitudinal FSW specimens. However, the fatigue strength of the FSW weld was higher than that of MIG and laser welds [141,142]. Typical S-N curves for FSW weld, laser weld, MIG weld, and base metal of 6005Al-T5 are shown in Fig. 32. The finer and uniform microstructure after FSW leads to better properties as compared to fusion (laser and MIG) welds. Second, surface quality of the FSW welds exerted a significant effect on the fatigue strength of the welds.

Hori et al. [140] reported that the fatigue strength of the FSW weld decreased with increasing tool traverse speed/rotation rate (n/v) ratio due to the increase of non-welded groove on the root side of the weld. However, when the non-welded groove was skimmed, the fatigue strength of the FSW weld remained unchanged by changing the n/v ratio. Furthermore, Bussu and Irving [142] reported that skimming 0.5 mm thick layer from both root and top sides removed all the profile irregularities and resulted in fatigue strength, of both transverse and longitudinal FSW specimens, comparable to that of the base metal. Similarly, Magnusson and Kallman [136] reported that the removal of 0.1-0.15 mm thick layer from top side by milling can result in a significant improvement in the fatigue strength of FSW welds. These observations suggest that the fatigue life is limited by surface crack nucleation and there are no inherent defects or internal flaws in successful FSW welds.

……Third, the effect of FSW parameters on the fatigue strength is complicated and no consistent trend is obtained so far. Hori et al. [140] reported that for a specific n/v ratio, the fatigue strength of the FSW weld was not affected by the tool traverse speed. However, Biallas et al. [40] observed that for a constant n/v ratio, the fatigue strength of FSW 2024Al-T3 welds with thickness of 1.6 and 4 mm was considerably enhanced with increasing tool rotation rate and traverse speed. The S-N data of 1.6 mm thick FSW weld made at a high tool rotation rate of 2400 rpm and a traverse speed of 240 mm/min were even within the scatter band of the base metal.

Fourth, low plasticity burnishing (LPB) after FSW can enhance the fatigue life of the FSW joints. Jayaraman et al. [145] reported that LPB processing increased the high cycle fatigue endurance of aluminum alloy FSW 2219Al-T8751 by 80% due to introduction of a deep surface layer of compressive residual stress. Also, the surface becomes highly polished after LPB and as noted earlier the fatigue life of FSW welds is limited by surface crack nucleation. Compressive residual stresses at surface and high-quality surface finish are desirable for good fatigue properties. Fifth, while the fatigue resistance of FSW specimens in air is inferior to that of the base metal, Pao et al. [89] reported that FSW 2519Al-T87 and base metal specimens have similar fatigue lives and fatigue thresholds in 3.5% NaCl solution. Again, the corrosion products at the surface are likely to influence the fatigue crack nucleation and the influence of FSW on corrosion adds to the complexity of corrosion-fatigue interaction. Overall, the fatigue results for FSW aluminum alloys are very encouraging.

5.3.2.2. Fatigue crack propagation behavior.

In recent years, several investigations were undertaken to evaluate the effect of FSW on the fatigue crack propagation behavior [89,92,137,138,146,147]. The investigated materials and specimens geometries used are summarized in Table 9. Donne et al. [137]

Table 9

A summary of materials and methods used for evaluating fatigue crack growth of FSW welds

Materials	Testing method	Reference
2024Al-T3	Compact tension	[137]
6013Al-T6	Compact tension; middle cracked tension	[137]
7050Al-T7451	Eccentrically loaded single edge tension	[102]
7050Al-T7451	Compact tension	[138]
2519Al-T87	Wedge-opening-load tension	[89]
2024Al-T351	Surface crack tension; compact tension	[147]

investigated the effect of weld imperfections and residual stresses on the fatigue crack propagation (FCP) in FSW 2024Al-T3 and 6013Al-T6 welds using compact tension specimens. Their study revealed following important observations. First, the quality of the FSW welds only exerted limited effects on the da/dN-DK curve. Second, at lower loads and lower R-ratio of 0.1, the FCP properties of the FSW welds were superior to that of the base metal for both 2024Al-T3 and 6013Al-T6, whereas at higher loads

or higher R-ratios of 0.7-0.8, base materials and FSW welds exhibited similar da/dN-DK behavior. This was attributed to the presence of compressive residual stresses at the crack tip region in the FSW welds, which decreases the effective stress intensity (DKeff) at the crack front. In this case, fatigue crack propagation rates at lower loads and lower R-ratio were apparently reduced due to reduced effective stress intensity. However, at higher loads or higher R-radios, the effect of the compressive residual stress becomes less important and similar base material and FSW da/dN-DK curves were achieved. Donne et al. [137] further showed that after subtracting the effect of the residual stress, the da/dN-DKeff curves of the base materials and the FSW welds overlapped. Third, specimen geometry exhibited a considerable effect on the FCP behavior of the FSW welds. Donne et al. [137] compared the da/dN-DK curves obtained by compact tension specimens and middle cracked tension specimens for both base material and FSW weld at a lower R-ratio of 0.1. While the base material curves overlapped, a large discrepancy was found in the case of the FSW welds. This was attributed to different distribution of the residual stresses in two specimens with different geometries.

The improvement in the FCP properties after FSW was further verified in FSW 2519Al-T87 and 2024Al-T351 by Pao et al. [89] and Bussu and Irving [147]. Pao et al. [89] reported that the mắt điểm hàn zone and HAZ of FSW 2519Al-T87 exhibited lower fatigue crack growth rates and higher fatigue crack growth threshold, DKth, at both R = 0.1 and 0.5, in air and in 3.5% NaCl solution, compared to the base metal. Furthermore, the FCP properties of the mắt điểm hàn zone were higher than those of the HAZ. Compared to the fatigue crack growth rates in air, the fatigue crack growth rates in 3.5% NaCl solution for the base metal, HAZ, and mắt điểm hàn zone, in the

intermediate and high DK regions, were about two times higher than those observed in air. However, at crack growth rates below about 10~8 m/cycle, DKth values in 3.5% NaCl solution were substantially higher than those in air because corrosion product wedging became increasingly prevalent and corrosion product induced crack closure progressively lowered the effective DK and eventually stopped the crack growth.

The DKth values obtained in both air and 3.5% NaCl solution are summarized in Table 10. Bussu and Irving [147] reported that crack growth behavior in the FSW 2024Al-T351 joints was generally dominated by the weld residual stress and that microstructure and hardness changes in the FSW welds had minor influence. Furthermore, they reported that fatigue crack growth rates in FSW 2024Al-T351 depended strongly on their location and orientation with respect to the đường trục hàn. However, in FSW weld

Table 10

Fatigue crack growth threshold, DKth (MPa m1/2) of FSW 2519Al and 7050Al alloys

……..

a FSW weld is in as-FSW + aging (121 °C/12 h) condition.
b FSW weld is in as-FSW + T6 condition.

which were mechanically stress relieved by application of 2% plastic strain, crack growth rates were almost identical to those of the base metal, irrespective of location and orientation.

On the other hand, in an investigation of fatigue-crack growth behavior of FSW 7050Al-T7451 in the as-FSW + T6 condition at the lower stress ratio of 0.33, Jata et al. [92] observed that the mắt điểm hàn zone had the lowest near-threshold resistance and the HAZ the highest near-threshold resistance (Table 10). At the higher stress ratio of 0.7, the differences in the fatigue crack growth rates of the base metal, mắt điểm hàn zone and HAZ were almost negligible.

Jata et al. [92] suggested that the decrease in fatigue crack growth resistance of the mắt điểm hàn zone was due to an intergranular failure mechanism and in the HAZ, residual stresses were more dominant than the microstructure improving the fatigue crack growth resistance. Similarly, Pao et al. [138] found that the HAZ of FSW 7050Al-T7451 in as- FSW + aged (121 °C/12 h) condition exhibited significantly lower fatigue-crack growth and much higher DKth at a stress ratio of 0.1 in both air and 3.5% NaCl solution. However, the FCP properties of the weld mắt điểm hàn region were basically identical to those of the base metal in both air and 3.5% NaCl solution. The low fatigue crack growth rate in the HAZ was attributed to residual stress and roughness induced crack closure. Furthermore, Pao et al. [138] reported a significant increase in the DKth values in 3.5% NaCl solution for the mắt điểm hàn zone, HAZ, and base metal (Table 10). This observation is similar to that in FSW 2519Al-T87 and attributed to the corrosion product wedging phenomenon.

5.3.3. Fracture toughness

It is usually accepted that all welded structures go into service with flaws ranging from volume defects like porosity, non-metallic inclusions to different planar defects like cracks induced by hydrogen or hot

tearing. There are standards for acceptability of the welds pertaining to different inspection codes. The non-acceptable flaws must be repaired before the weld is put into service. Most existing codes cater toward weldments made by conventional welding techniques. FSW is generally found to produce defect-free welds. However, no established code exists so far for FSW. Considering potential applications of FSW, there is a critical need for proper evaluation of the fracture behavior of the friction stir welds. The most commonly used parameters are the crack tip intensity factors (K) for linear elastic loading, and the J integral or the crack opening displacement (CTOD) for elastic-plastic loading [148].

Since the first international symposium on friction stir welding in 1999, several investigations have been conducted to evaluate the effect of FSW on the fracture toughness [40,134,135,149-152]. The materials investigated and the methods used to measure the fracture toughness are summarized in

Table 11
A summary of materials and methods used for evaluating fracture toughness of FSW welds
Materials Testing method References
……..

Table 12

Fracture toughness (CTOD(d5)m, mm) of FSW welds and respective base metals obtained by means of compact tension (after von Strombeck et al. [135])
……..

Table 11. von Strombeck et al. [135] investigated the fracture toughness behavior of several FSW aluminum alloy by means of compact tension (CT) tests. The fracture toughness values in term of d5 CTOD are summarized in Table 12. It is noted from Table 12 that the fracture toughness values of FSW 5005Al-H14, 6061Al-T6 and 7020Al-T6 are much higher than that of respective base metals, whereas FSW 2024Al-T6 exhibited a slightly reduced fracture toughness compared to the base metal (Table 12). Further, Table 12 demonstrates that the fracture toughness of the mắt điểm hàn zone was superior to that of the TMAZ/HAZ region for all alloys.

Recently, Dawes et al. [134] measured the fracture toughness of FSW 2014Al-T651, 7075Al-RRA and 5083Al-O by means of single edge notched three-point bend tests as per ASTM E 399-90 and E 1820-99. The CTOD and J values indicate that fracture toughness of the FSW welds are considerably higher than that of the respective base metals for all three alloys (Table 13). The results ofDawesetal. [134] show that the fracture toughness of the mắt điểm hàn zone is not always higher than that of the HAZ/TMAZ region, which is different from the results reported by von Strombeck et al. [135]. More recently, Kroninger and Reynolds [152] studied the R-curve behavior of FSW 2195Al-T8 welds by using compact tension specimens and compared it

Table 13
Fracture toughness of FSW welds and respective base metals near the onset of stable crack extension obtained by means of single edge notched bend (after Dawes et al. [134])

TMAZ 0.5 mm from the edge of weld mắt điểm hàn on advancing side 0.051 17 …….	[redacted]
TMAZ 0.5 mm from the edge of weld mắt điểm hàn on advancing side 0.036 17.2 ……...	[redacted]
a do.2BL and Jo.2BL are very similar to the dIc and JIc fracture toughness, respectively, in the ASTM E 1820-99 test method. b RRA refers to retrogression and re-aging (rapid heating to 220 °C, kept for 5 min, cold water quenched, re-aged at 120 °C for 24 h).	[redacted]
Fig. 33. Representative R—curves for all 2195A1 FSW crack planes, 2195 base metal, and centerline crack in the VPPA weld (after Kroninger and Reynolds [152]).	Hình 33. Đường cong R biểu diễncho tất cả các mặt phẳng nứt 2195A1 FSW, kim loại cơ bản (kim loại gốc, kim loại nền) 2195, và vết nứt trục đường trong mối hàn VPPA (theo Kroninger và Reynolds [152]).